Combustion and Flame 233 (2021) 111589

Contents lists available at ScienceDirect

Combustion and Flame

journal homepage: www.elsevier.com/locate/combustflame

Experimental investigation of the lift-off height and soot formation of a spray flame for different co-flow conditions and fuels

Jaime Gimeno*, Pedro Martí-Aldaraví, Marcos Carreres, Santiago Cardona

CMT Motores Termicos, Universitat Politécnica de Valéncia, Spain

ARTICLE INFO

Article history:
Received 25 August 2020
Revised 22 June 2021
Accepted 27 June 2021

Keywords:
Spray flame
OH* chemiluminescence
Diffused back-illumination extinction
Flame lift-off height
Soot formation
Co-flow velocity

ABSTRACT

Since the combustion process in spray flames is a highly complex multi-phase phenomenon, which involves several simultaneous processes such as atomization, vaporization, and chemical kinetics, it is still not fully understood. In the present work, an experimental investigation has been performed for three different hydrocarbon fuels (n-Heptane, n-Decane, n-Dodecane), in order to understand the effect of varying co-flow conditions, fuel mass flow rate, and fuel type on both the flame lift-off height and soot formation. The fuels were injected through a hollow-cone spray injector, with a nominal spray cone angle of 80° and orifice diameter of 120μm in an annular non-swirled preheated air co-flow. The flame lift-off height was determined by recording the OH* chemiluminescence, whereas soot formation has been determined through the color diffused back-illumination extinction technique. From the results, it has been observed for a certain fuel that the flame lift-off height is mainly controlled by the co-flow velocity and air co-flow temperature. The results also show that the fuel that yields largest droplet size and that possesses the lowest volatility exhibits the highest flame lift-off height. Furthermore, the results evidence a strong influence of the co-flow velocity on the soot formation. With an increase in co-flow velocity, the flame lift-off height is increased and so the amount of air entrainment, leading to a less rich reaction zone just downstream of the lift-off height, which in turn results in less soot formation. Finally, the comparison among different fuels shows that their differences in soot formation are likely related to fuel sooting tendency. This property, in turn, depends on the fuel molecular structure playing an important role on its determination.

1. Introduction

The understanding of soot formation in spray flames during the combustion process is an essential factor to control soot emissions from the burning of fossil fuels for various power generation and propulsion technologies. These applications adversely affect the environment, so that the laws about unhealthy exhaust emissions have become more stringent. Researchers have studied these processes trying to reduce the pollutant emissions (especially soot particles) through continuous improvements in both combustion processes and combustor design. To these aims, it is necessary to develop experimental techniques, particularly nonintrusive optical techniques. Well-established techniques are usually based on light extinction and scattering as explained in [13] and references therein.

Due to the fact that soot formation has a long dependency on the flame lift-off height [67], it is extremely important to understand the characteristics of lifted flames and their blow-off features under different conditions of co-flow velocity, fuel flow rate, and air temperature. During the last two decades, many authors have widely studied flames from gaseous fuels and combustor configurations [2,11,20,96]. Although a substantial amount of work on the behavior of gaseous lifted flames has been reported in the literature (as reviewed by [39,42]), only a few works have been reported for liquid fuels characterizing the flame lift-off and blow-off characteristics with different co-flow conditions [4,49,72,91]. The burning process of liquid fuels becomes much more complex because it involves many sub-processes such as atomization, evaporation, mixture formation, and subsequent combustion reaction [4,23,24,82,83]. The investigations on lift-off

* Corresponding author.
E-mail address: jaigigar@mot.upv.es (J. Gimeno).

https://doi.org/10.1016/j.combustflame.2021.111589

Nomenclature

CCD	charge-coupled device
DBI	diffused back-illumination
fps	frames per second
FWHM	full width at half maximum
TSI	threshold soot index
YSI	yield soot index
H	hydrogen atom
ICCD	intensified charge-coupled device
LED	light-emitting diode
LEM	laser extinction method
LII	laser-induced incandescence
PLIF	planar laser-induced fluorescence
PID	proportional integral derivative
f_v	soot volume fraction
I	measured transmitted intensity
I_f	light from the flame
I_0	reference illumination
k_e	dimensionless optical extinction coefficient
KL	optical thickness related to soot
LOH	lift-off height
m	refractive index
$T_{co-flow}$	air co-flow temperature
$ø_{air}$	air outlet diameter
V_r	resultant mixture velocity
$V_{droplet}$	droplet ejection velocity
S_L	laminar flame speed
S_{spray}	flame speed
$V_{co-flow}$	co-flow velocity
KA	light attenuation in a sheet-of-sight
KV	total light attenuation
L	path length
K	dimesional extinction coefficient
SMD	Sauter mean diameter
RDG	Rayleigh-Debye-Gans theory
TEM	transmission electron microscope
UV	ultraviolet
α_{sa}	scattering-to-absorption
ϕ_{global}	global equivalence ratio
ρ_{air}	air density
ρ_l	fuel density
σ_l	liquid surface tension
ν_l	kinematic viscosity
μ_l	dynamic viscosity

flames are also important to understand the flame dynamics inside gas turbines or applications with liquid fuel jets. Preliminary works on the characteristics of spray flames have been reported by Akamatsu et al. [1,81,89]. Chiu et al. [15] have observed that when liquid fuel is injected, a dense droplet cloud is formed near the nozzle exit (distance between the droplets is less than the droplet diameter), and the entrainment of surrounding air near the fuel nozzle is very small. Additionally, Chiu and Lin [16] reported that, as the co-flow velocity is increased, the droplets are transported downstream, the distance between droplets being increased, which makes the cloud less dense and allows to increase the air entrainment from surroundings.

Previous studies on lifted spray flames suggested that a structure similar to that of a gaseous diffusion flame is formed in spray flames since fuel droplets evaporate close to the fuel nozzle so that only a single reaction zone is present [58,59]. Nevertheless, recent studies supported that spray flames can exhibit a double structure, originating at the leading edge of the stabilized flame and diverging in the downstream location [3,12,24,46,49]. Moreover, it has been reported that in reacting sprays, a flame stabilizes when small droplets are available (to readily provide a mixture of fuel vapor and air) along with large-scale flow structures. This enhances the mixing of the fuel vapor with the entrained air [72]. Several authors performed the study on lifted spray flames with and without co-flow and reported that without co-flow, the flame exhibits a single flame structure. The addition of low-speed co-flow, on the other hand, lifts the flame and leads to increased entrainment of air in the spray [49,50]. The presence of large quantities of oxidizer within the fuel spray creates a unique double reaction zone structure.

Experimental studies by Reddy et al. [72] investigated lifted spray flames for a range of co-flow conditions, varying the co-flow temperature and testing different nitrogen dilutions. They reported that increasing the co-flow temperature decreases the flame lift-off height, as a result of enhancing the fuel vaporization rate. In a related work, Weinberg and Greenberg [91,92] investigated mathematically the flame lift-off height of a laminar jet spray diffusion flame, providing a discussion on different flame scenarios related to variation in droplet size and initial spray polydispersity. Recently, Alsulami et al. [4] have conducted an experimental investigation for different hydrocarbon fuels to study the role of the atomization process on flame stability (flame lift-off height and blowout limit), remarking the importance of considering both the physical properties (which can influence atomization, vaporization and the mixing process) and the fuel's chemical reactivity when projecting the performance of the fuel.

Soot formation in spray flames has been extensively studied too [18,93]. Previous observations have shown that soot particles become less reactive for soot surface growth as the residence time in flames increases. Frenklach and Wang [25] reported that this reduced reactivity to soot growth is caused by reduced concentrations of Hydrogen as flow temperatures decrease thanks to radiative heat losses to the surroundings. Some authors have suggested that the droplet size distribution of the fuel spray has a notable influence on combustion behavior [8,30] and hence soot formation [31,97]. Soot formation is a complex phenomena in combustion, involving interactions between combustion chemistry, fluid mechanics, mass/heat transport, and particle dynamics. Despite the great effort to fully understand this phenomenon, several details remain unknown [85,88]. In addition, the conditions for soot formation can be very different among experimental setups. Therefore, conclusions regarding the sooting processes obtained from one configuration may not be directly applicable to others. Soot formed in the fuel-rich region of a normal co-flow flame is always convected downstream towards the high temperature flame front, where fuel and oxidizer are mixed stoichiometrically. As a result, oxidation of soot by oxygen and hydroxyl radicals is inevitable. In fact, the widely referred smoke point condition is a critical condition where soot formation is balanced just by its oxidation [7,79]. Recently, several studies have been performed in order to investigate experimentally the soot formation in turbulent spray flames [52,53,86]. Wang et al. [86] investigated two Jet A-1/ air spray flames using laser-induced incandescence (LII) for soot concentrations and stereoscopic particle image velocimetry for velocity fields, reporting that the soot distribution in liquid-fueled swirl-stabilized flames is drastically different from their gas-fueled counterparts. Mulla and Renou [53] investigated experimentally soot formation in a turbulent n-Heptane spray flame through quantitative soot volume fraction (f_v) using LII and planar laser-induced fluorescence (PLIFT) to measure simultaneously the soot-precursor (PAH) and flame-front (OH), contributing with a soot database for model validations, identification of soot onset

and oxidation zones, and analysis of soot-PAH correlations at different stages of soot maturity.

As was mentioned earlier, spray combustion has been widely studied in the literature. Jenny et al. [38] made recently an extensive review of breakup, dispersion, evaporation, mixing and combustion regimes in spray combustion. The presence of droplets poses a difficulty to experiments, even though several classical and new techniques can perform accurate and reliable measurements. Although several authors have determined the lift-off height directly recording the flame through a CCD camera [35,36,72,87], OH* chemiluminescence has demonstrated to be an excellent marker to measure lift-off height. The reason is that it occurs primarily under high-temperature stoichiometric combustion [34], and it is present at the flame stabilization region in lifted turbulent-diffusion flames [66]. Moreover, OH* radicals have the strongest emittance band at 306 nm, which is distant from the soot incandescent wavelength avoiding to mask it. OH* emittance band is recorded by an intensified charge-coupled device (ICCD) camera equipped with a UV lens and a narrow band-pass filter of 310 nm to capture the low-intensity signal from the combustion. This methodology has been implemented in many studies [63,65,67–69,76]. On the other hand, soot has been studied throughout both laser and optical techniques. LII and laser extinction measurement (LEM) represent the most common techniques employed in situ for characterization of soot volume fraction (f_v) [14,17,67]. Even though the single-point light-extinction method is accepted due to its simplicity and accuracy, obtaining a 2D soot distribution by using a single-point measurement is an ardous task. A more efficient method is to record the full-field light extinction by a whole soot cloud using an expanded light source and a focal-plane imaging device. Two-color techniques have also been used lately to measure soot in diesel fuel jets [62,98]. Nakakita et al. [56] used a back-illumination method to study the soot clouds and highlighted its advantage. Nowadays, this technique has good acceptance among researchers to study soot formation. This fact has led to an extensive implementation and improvement [47,48,63,77,78,80]. Manin et al. [47] developed a high-speed back-illumination extinction imaging technique. This new diagnostic was validated by concurrently measuring the path-averaged optical thickness (KL) using LEM. Thanks to the implemented optical arrangement, the effects of beam steering on the measured extinction were reduced. Finally, their results allowed them to conclude that shorter visible wavelengths are preferred to measure soot concentration.

Although a significant number of researches have been conducted in spray flames and the soot formation in them, as was detailed previously, spray flame is a complex multi-phase phenomenon, and its fundamental physics is not completely understood. Therefore, the current work aims to investigate experimentally the effect of fuel properties on the flame lift-off height and soot formation over a wide range of operating conditions using a pressure-swirl injector with a considerably smaller injector orifice diameter than ones reported in the literature. Co-flow velocities were relatively high, the burner geometry configuration is different and the use of two different air outlet diameters allowed observing the effect of the global equivalence ratio on both flame lift-off height and soot formation at the same operating conditions. Furthermore, thanks to the high number of operating conditions tested and combined with diverse configurations enable the observation and explanation of some trends non-reported by other authors. This study also contributes to removing uncertainties related to different experimental test rigs, visualization techniques and employed hardware. Finally, this study provides an experimental correlation for lift-off length using the parameters evaluated and clear explanations for several observed trends. In the present work, the effect of co-flow conditions, fuel mass flow rate and fuel type on both flame lift-off height and soot formation has been experimentally studied for three single liquid hydrocarbon fuels, namely n-Heptane, n-Decane and n-Dodecane. A commercially available pressure-swirl fuel nozzle (hollow cone pattern) is used due to its reliability, good quality atomization, simplicity of construction and low pumping power requirements [22,29]. Following the present introduction, this document is formed of three additional sections. The next section discusses the experimental facility, providing details on the optical setup, image processing methodology and testing conditions on which the experiments have been performed. The third section presents the results of OH* chemiluminescence and optical extinction in a spray flame surrounded by different co-flow conditions. The last section summarizes the work performed and the main findings after its execution.

2. Material and methods

This section details the facility used to carry out the experiments of spray flame characterization, giving details on the optical setups, the image processing methodology for each applied technique and the operating conditions tested. The test rig has been designed to supply high-airflow at high-temperature, allowing a wide range of co-flow conditions to be evaluated. The test section where the spray flame takes place is fully accessed optically, thus enabling to easily set up different optical techniques, even simultaneously.

2.1. High-flow and high-temperature facility

Fig. 1 shows the schematic layout of the present experimental setup used to study the behavior of the atomization and combustion processes in spray flames at atmospheric conditions. Air co-flow is supplied through a centrifugal blower with an air blowing capacity of 0–400 kg h^{-1} and measured through a flow meter. The change in flow direction was carried out through a series of elements such as a volute, guiding vanes and a final section filled with stainless steel spheres. These elements were coupled to the air pipeline before the combustion zone, ensuring an airflow with a uniform velocity profile. A 15 kW electric heater has been disposed at the air pipeline to increase the air temperature up to 673 K, allowing to study its effect on the combustion and atomization processes. The air co-flow temperature is measured with K-type thermocouples at different locations and controlled by a PID module. The burner is located after the electric heater and a non-swirled flow configuration was chosen to perform the experiments.

The fuel injection system mostly consists of a pressurized vessel (2L capacity) that can be pressurized up to 5 MPa through a nitrogen bottle. Pressure is maintained by through a pressure regulator. The vessel has been provided with multiple input connection ports, allowing to attach different sensors (e.g., thermocouples, pressure sensor), and valves to it. A safety valve also has been installed to prevent an over-pressure in the system, releasing the pressure when it reaches 7 MPa. An electronic Coriolis mass flow meter (Bronkhorst, CORI-FLOW) has been arranged at the fuel pipeline for an accurate measurement of the fuel mass flow rate. Additionally, two electro-valves were provided upstream of the injector to control the fluid flow through it, cutting it off when necessary to avoid injector's dribble. The fuel is injected through a hollow cone spray injector with a spray angle of 80° and a mass flow rate of 0.57 kg min^{-1} at 1 MPa for a calibration fluid (ISO 4113). The orifice diameter is 120μm and was measured using x-ray tomography.

The burner is fully accessed optically, allowing a direct visualization of the spray flame. Different optical techniques can be used simultaneously. The design is modular and can be easily rearranged to simulate various air co-flow configurations, e.g., in

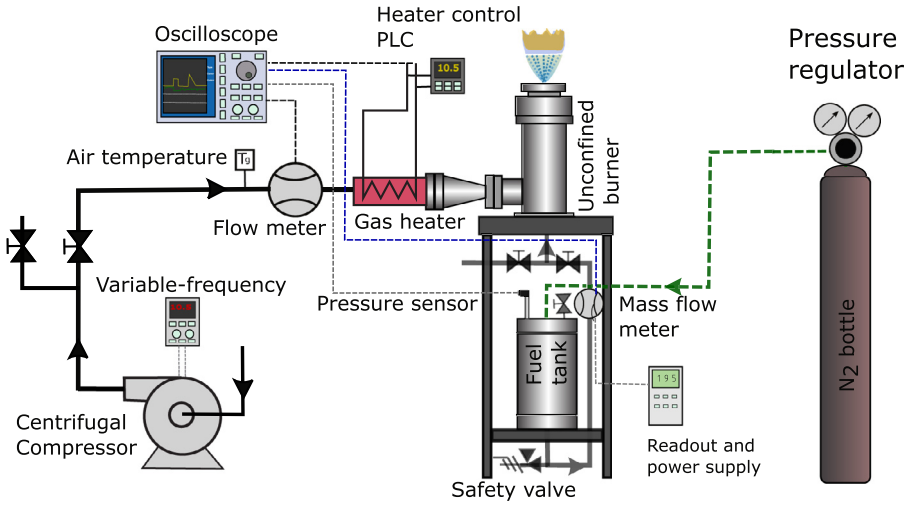

Fig. 1. Schematic diagram of the experimental setup for lifted spray flames.

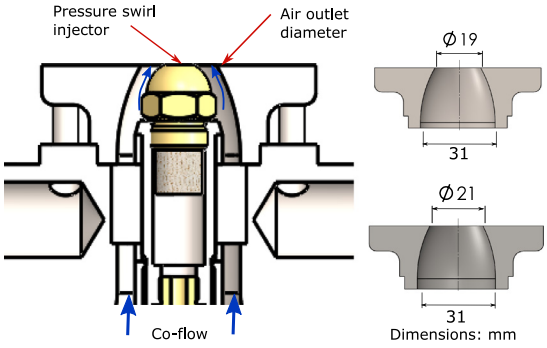

Fig. 2. Cross-sections of both atmospheric burner and air outlet diameters.

this work, two outlet diameters were tested. Furthermore, a cross-section of insulating material was utilized between the external housing and the internal flow duct to avoid heat losses. Finally, the injector was mounted in a way that it allows the whole spray to be registered from the nozzle tip, as shown in Fig. 2.

2.2. Optical techniques and setup

2.2.1. Chemiluminescence

Chemiluminescence is defined as a light emission phenomenon resulting from a chemical reaction, commonly associated with a release of heat. This technique has been extensively used in combustion research since OH radicals emit luminescence when they decay at their ground state. This luminescence can be captured and used in several diagnostics such as detection of high-temperature regions and estimations of the equivalence ratio [45,60,61]. Thus, with the suitable optical setup, OH^* chemiluminescence is an excellent marker to determine the flame lift-off height [34]. Therefore, an ICCD Andor iStar camera equipped with a 100mm f/2.9 UV-capable lens and with the corresponding filter for OH^* chemiluminescence (narrow band-pass filter of 310 ± 5nm has been used). The filter was arranged shaping a slight angle to the optical axis to avoid interfering with the diffuser used for DBI technique, as shown in a simplified schematic diagram in Fig. 3.

2.2.2. Diffused back-illumination extinction

The principle of this technique is based on measuring the amount of light attenuated or extinguished by the interference of some features like droplets, soot particles, etc. It considers the liquid or soot particles as the dark silhouette of the flame when the background is illuminated by a diffused light. In this work, the diffused back-illumination extinction technique is used to measure the light attenuation by the soot cloud. However, the images recorded through this technique also captured the attenuation generated by the droplets existing at the region located upstream from the flame stabilization point. This attenuation will not be treated in this study. Several measurements have been implemented to prevent the light from the flame to get to the camera. First, a color light-emitting diode (LED) light source was used together with a narrow band-pass filter with the same wavelength. A short light-pulse was set, allowing to reduce the exposure time of the camera, thus recording less light from the flame. Despite the measures implemented to cut-off the broad-band intensity from the flame, part of this intensity is recorded by the camera, forcing to remove it in the image processing step thanks to the frames recorded with LED-off. Finally, 600 frames with LED-on and 600 frames with LED-off (recorded in successive batches of 20 frames as depicted in Fig. 4) were averaged to obtain proper mean images of the flame. Note that the number of frames was examined in order to minimize the error when calculating the mean image of *KL*.

The optical setup for the diffused back-illumination extinction diagnostic technique is formed mainly of a LED as an illumination source and a high-speed camera (Photron SAZ) on opposing sides of the spray flame in a line-of-sight arrangement, as shown in a simplified schematic layout in Fig. 3. A blue LED unit centered at 460nm was mounted and the LED's rays were directed to a Fresnel lens (focal length of 67mm). Then a big square diffuser was placed in such a manner that the diffused background created was relatively large (more than 100 mm in diameter) and uniform at the optical test plane of the spray flame. The LED unit can produce short and high-power pulses of light and a high rate of repetition. The duration of the pulse was set at 20 μs as a compromise between intensity illumination and camera speed.

The camera was equipped with a 24–70 mm Sigma lens and was set with an acquisition rate of 250 fps and an exposure time of 40 μs in order to fully acquire the period of the LED illumination. In order to effectively capture the extinction signals, a filter must be placed in front of the camera objective. Therefore, a bandpass filter that transmits from 455nm to 465nm (measured at FWHM) was selected, which rejects most of the broadband luminosity from the flame. The filter and LED unit have been placed on a motorized translation stage to align them. Details about the optical setups are presented in Table 1.

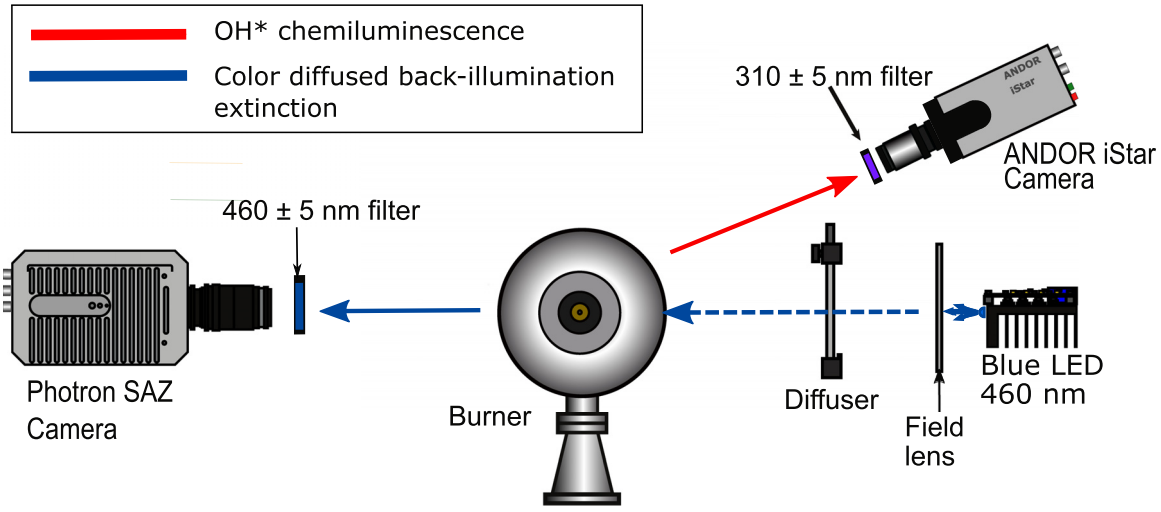

Fig. 3. Schematic top view of the optical setup used for OH* chemiluminescence (red path) and microscopic diffused back-illumination (blue path). (For interpretation of the references to colour in this figure legend, the reader is referred to the web version of this article.)

Table 1
Details of the optical setup for both DBI and OH* Chemiluminescence techniques.

	DBI	OH* Chemiluminescence
Camera	Photron SAZ	Andor iStar
Camera lens	Sigma 24–70 mm f/2.8	100 mm f/2.9 UV
LED pulse duration (μs)	20	-
Filter CWL (nm)	460	310
Frame rate (fps)	1000	30*
Field of view (pixels)	1024x1024	1024x1024
Exposure (μs)	40	3×10^4
Pixel-mm ratio	7.45	9.45
Repetitions	600 LED-on - 600 LED-off	30

* Per operating point.

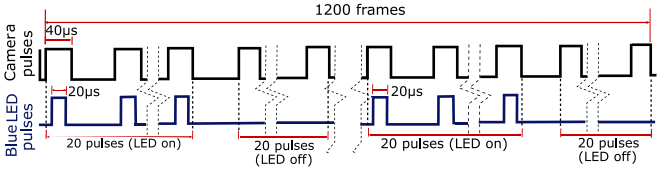

Fig. 4. Sketch of the camera and LED pulses. Movies consist of successive batches of 20 frames with LED-on and the following 20 frames with LED-off up to record 1200 frames.

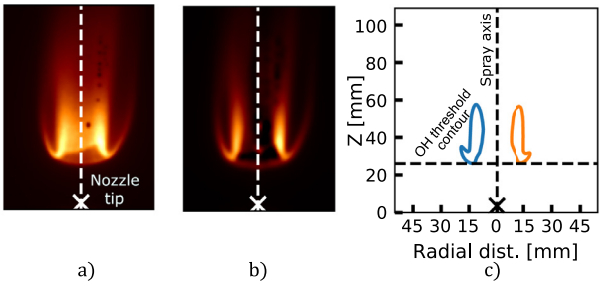

Fig. 5. (a) OH* chemiluminescence raw image, (b) OH* chemiluminescence image after computing the Inverse Abel Transform, using a Basex method, (c) Contour of the flame at central plane (image b) with a set threshold. The frame shown is a n-Dodecane flame with an air co-flow temperature of 328 K, for an air mass flow of 11.9 kg h^{-1} and fuel mass flow of 135 mg s^{-1}.

2.3. Image processing

This section presents the processing methodology for the images recorded through the OH* chemiluminescence and color diffused back-illumination extinction techniques. The methods implemented to analyze the combustion properties of the flame at the central cross-section are also described next.

2.3.1. Flame lift-off height

The field of species concentration can be recorded by viewing the reacting zone through an appropriate optical band-pass filter, allowing only the spectrum of light emitted by the species of interest to pass. Nevertheless, such an image contains the concentration of the entire volume, since each pixel captures the integrated light from the entire volume passing through its line-of-sight. In order to resolve an axisymmetric integrated line-of-sight data distribution to one at a given azimuthal plane, the mathematical Inverse Abel Transform was used [84]. This method takes a 2D projection and reconstructs a slice of the cylindrically symmetric 3D distribution as shown in Fig. 5. Since the spray flame is not completely axisymmetric, the Abel transform was computed for each half of the image separately, as shown in Fig. 5b. Fig. 5 also shows that the flame shape is well defined, suggesting that the effects of the non-axisymmetry do not seem to modify the flame morphology. The inverse Abel method plays an important role in analyzing the projection flames [9,18,19,70,84]. Therefore, the processing stage started by calculating the Abel inversion for each recorded frame of OH* chemiluminescence.

The flame lift-off height is determined by averaging 30 OH* chemiluminescence frames per operating condition. These frames were captured through an ICCD camera for each stabilized period

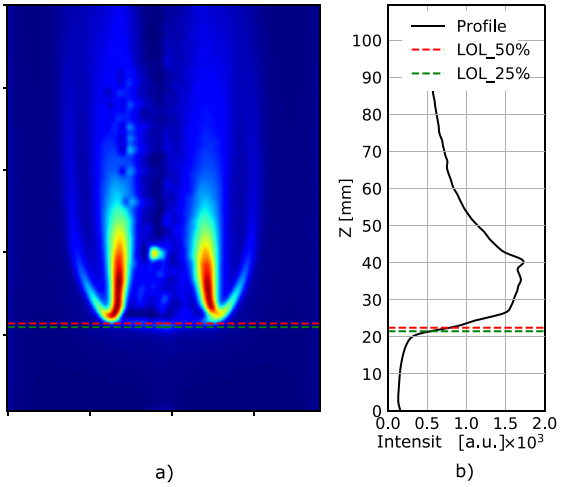

Fig. 6. (a) OH* chemiluminescence image after computing the Inverse Abel Transform, using a Basex method, (b) Intensity profile of averaged flame, dashed lines represent flame lift-off measured with both thresholds. The frame shown is a n-Decane flame with an air co-flow temperature of 328 K, for an air mass flow of 13.8 kg h^{-1} and fuel mass flow of 189mg s^{-1}.

of the combustion in order to obtain a proper mean image of the flame. The exposure time of the camera was set at 0.3s, integrating the flame radiation for a long time gap thus averaging turbulent fluctuations of the flame lift-off height. The images then represent spatial and temporal averages of radiation. The processing methodology to measure the flame lift-off height has been done following the methodology proposed by Siebers [75] for diesel fuel jets. After computing the Abel transform and averaging all repetitions, both sides of the resultant image are averaged and filtered with a Gaussian filter. Then, the mean intensity is traced for each height position, generating an intensity profile of the flame. Finally, two thresholds are defined as 25% and 50% of the difference between the first levelling-off peak and background noise. The background noise is calculated by averaging the first 7mm from the nozzle tip, where no flame is present. The flame lift-off height is defined as the distance between the nozzle tip and the closest point in the flame above the calculated thresholds as shown in Fig. 6b. Even though no large differences in *LOH* were found when processing with the two chosen thresholds, the results presented in the next section correspond to the threshold of 25%, which is slightly more sensitive to the intensity changes.

2.3.2. Soot measurements through diffused back-illumination extinction

As an extinction-based diagnostic, the soot volume fraction is related to the amount of light that has been absorbed or scattered by the soot cloud. The extinction can be calculated for each frame using the Beer-Lambert law as presented in Eq. (1).

$$\frac{I - I_f}{I_0} = e^{-KL} \tag{1}$$

where I is the pixel-wise intensity distribution of the current frame that considers attenuation from the soot (LED-on), I_f accounts for the light emitted by the flame for the same time step (LED-off), and I_0 is the reference illumination calculated as the average of the images before the injection event. K is the dimensional extinction coefficient and L is the height of the path through the soot cloud. Thus, conditions with higher soot concentrations present a higher KL factor, although it is limited to the dynamic range of the images recorded. A graphic explanation on how the KL was calculated is presented in Fig. 7, the optical thickness being proportional to the soot concentration along the line-of-sight of the extinction measurement.

It is important to note that this technique has some limitations. One of these limitations is that some cameras have problems with fully resetting the sensor after the readout process when recording at relatively high speeds. For these reasons, the movies were recorded in batches of 20 repetitions until recording 1200 frames, then averaging them and removing the first frame after each batch to avoid this issue. Manin et al. [47] studied this effect, highlighting the complexity of the process and the difficulty to quantify it.

Quantitative soot measurements as a measure of the light extinction can be dominated by large uncertainties. Among them, the calculation of the dimensionless optical extinction coefficient (k_e) can be mentioned. This coefficient has considerable control over the result of soot volume fraction (f_v). This uncertainty comes from the dependence on a high number of parameters (e.g., soot morphology, complex refractive index of soot, fuel sooting propensities) and the complexity to measure them experimentally. For these reasons, the present work presents the results related to the light extinction measurements in terms of the dimensional extinction coefficient, K.

The dimensional extinction coefficient was calculated through the Abel Transform of KL image results, for which several methods have been developed. This makes it challenging to select the proper method for a specific application. Therefore, three methods (`Basex`,`Onion peeling`,`Three points`) out of the eight methods implemented in the PyAbel open source package for Python [33] were compared at random height. They are depicted as a yellow line in Fig. 8a and are commonly used in the analysis of flames and plasma plumes [27]. Firstly, the inverse transform is computed at this height, i.e. it takes a 2D projection of the object to calculate a slice of the 3D object (Fig. 8b). Secondly, the forward transform is calculated for the previous step, i.e. to transform a slice of a 3D object into a 2D projection of the object (Fig. 8c). For this work, the `Basex` method was chosen and the "Tikhonov regularization" was set to 50, which provides reasonable noise suppression while still preserving the fine features in the image, as depicted in Fig. 8. Furthermore, this method is computationally cheap.

After computing the Abel transform, a slice of the flame at the central plane is obtained. In this slice, the light attenuation by both liquid phase and soot particles can be appreciated, as shown in Fig. 9a. Since we are only interested in analyzing the combustion zone, the following methodology was used to find the border between the two zones through thresholding method: First, a threshold was set to split the image into two zones (Fig. 9b). Then, an algorithm was performed in order to find the border between them. Note that this threshold is not fixed and was calculated for each tested condition because the intensity and location of these zones vary, but both zones are well defined in all cases. Finally, the image was masked in order to only maintain the combustion zone (Fig. 9c).

2.4. Test conditions

In the present work, all experiments were performed for three different hydrocarbon fuels (n-Heptane, n-Decane and n-Dodecane) injected through a commercially available hollow-cone spray injector. Table 2 summarizes the fuel properties relevant to this study. The fuels were chosen to cover a good range of physical properties, such as density, surface tension and viscosity, which influence the spray characteristic (i.e., SMD). Additionally, boiling temperature and vapor pressure are included, which play an important role in the vaporization of the fuel. n-Heptane is the most volatile fuel, followed by n-Decane and then n-Dodecane, which

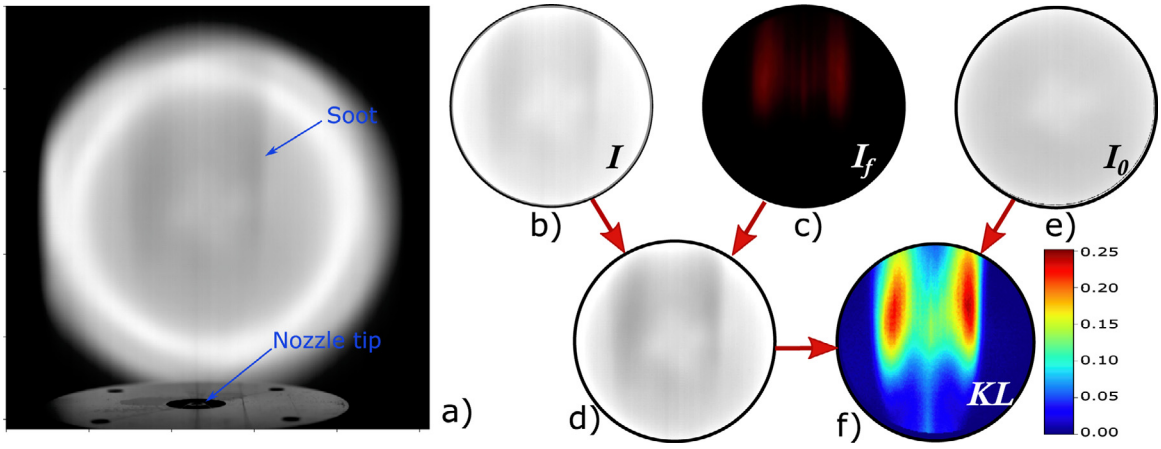

Fig. 7. (a) Raw image, (b) Light attenuation by the soot cloud, I, (c) Light emitted by the flame, I_f, (d) It is the image resulting of the subtraction image (c) from (b), i.e, real attenuation, (e) Reference illumination, I_0, (f) Optical thickness. Frames (b), (c) and (d) same intensity level. The frame shown is a n-Dodecane flame with an air co-flow temperature of 328 K, for an air mass flow of 11.9 kg h^{-1} and fuel mass flow of 135 mg s^{-1}.

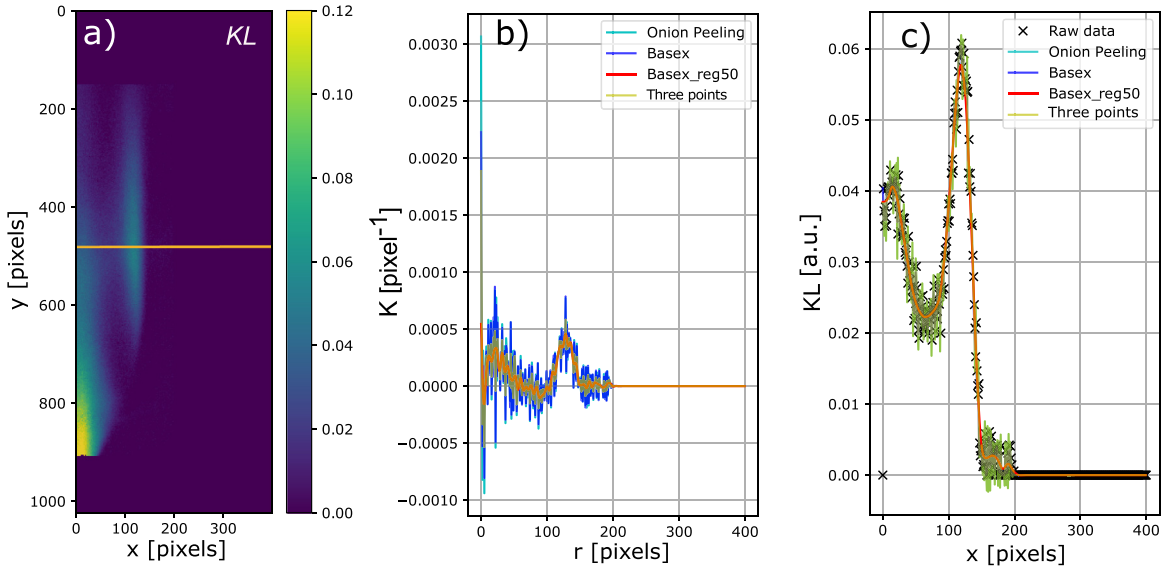

Fig. 8. (a) Soot attenuation presented in terms of the optical thickness (KL), yellow line represents the height to compute the Abel transform, (b) Inverse transform computed at the chosen height, (c) Forward transform of the inverse results presented in (b). The frame shown is a n-Dodecane flame with an co-flow temperature of 328K, for an injection pressure of 0.1 MPa, an air mass flow of 11.9 kg h^{-1} and fuel mass flow of 135 mg s^{-1}. (For interpretation of the references to colour in this figure legend, the reader is referred to the web version of this article.)

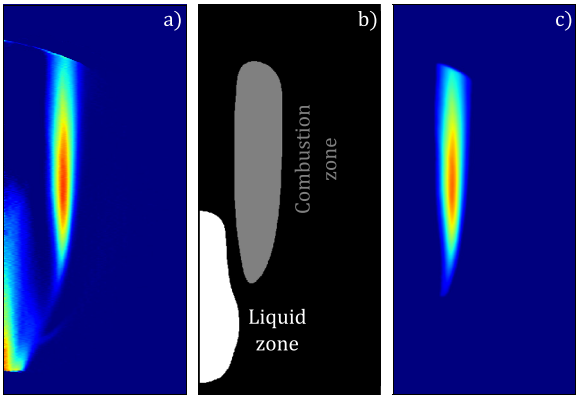

Fig. 9. Example of the segmentation algorithm, (a) attenuation by both liquid phase and soot particles, (b) classification of combustion and liquid zones, (c) attenuation by soot particles. The frame shown is a n-Decane flame with an air co-flow temperature of 328 K, for an air mass flow of 11.9 kg h^{-1} and fuel mass flow of 135 mg s^{-1}.

Table 2
Physical and chemical properties of the fuels. Most of the properties were extracted from the NIST database at normal temperature an pressure (i.e., 293.15 K and 1 atm) [44]. Laminar flame speed values were measured by previous works at 400 K, at 1 atm, and stoichiometric equivalence ratio [40,55].

Properties	n-Heptane	n-Decane	n-Dodecane
Formula	C_7H_{16}	$C_{10}H_{22}$	$C_{12}H_{26}$
Density (ρ_l) [kg m^{-3}]	683.94	730.53	749.5
Dynamic viscosity (μ_l) [Pa s]	0.00041	0.00091	0.00149
Surface tension (σ_l) [N m^{-1}]	0.0206[a]	0.0238[a]	0.0254[a]
Normal Boiling point [K]	371.53	447.27	489.3
P_v [kPa]	160[b]	16,5[b]	3.8[b]
S_L[m s^{-1}]	0.6413	0.6410	0.6405

[a] Along the saturation curve, [b] At 387 K.

has a boiling point that is more than 100°C higher than the n-Heptane fuel and 20°C higher than the n-Decane fuel. The reactivity of the fuel is marked by the laminar flame speed (S_L), which can impact the flame stability, especially flame lift-off. Even though S_L values are close to each other, the fuel that exhibits a lower reactivity is n-Dodecane.

Table 3
Test conditions matrix.

Parameter	Value
Fuel mass flow rate ($\dot{m}_l$)[mg s^{-1}]	(130, 159, 187.6)[a] (130.8, 159.83, 188.89)[b] (131.23, 160.4, 189.54)[c]
Air mass flow rate ($\dot{m}_{air}$) [kg h^{-1}]	11.9 - 13.6 - 15.6
Global equivalence ratio (ϕ_{global})	0.45, 0.52,0.55, 0.6, 0.63, 0.65, 0.73, 0.75, 0.86
Co-flow temperature ($T_{co-flow}$) [K]	328 - 373 - 423
Air outlet diameter ($\o_{outlet}$)[mm]	19 and 21

[a] n-Heptane, [b] n-Decane, [c] n-Dodecane

The test plan is presented in Table 3, consisting of three air temperature (328, 373 and 423K) and nine global equivalence ratios (which are directly related to air mass flow, injection pressure and fuel type) for each air outlet diameter. The global equivalence ratio (ϕ_{global}) is defined as the ratio of the actual fuel/air ratio to the stoichiometric fuel/air ratio, as shown in Eq. (2). It was varied in a range of fuel-poor conditions from 0.45 to 0.86. Note that the fuel mass flow rate is controlled by the injection pressure.

$$\phi_{global} = \frac{\frac{\dot{m}_l}{\dot{m}_{air}}}{\left(\frac{\dot{m}_l}{\dot{m}_{air}}\right)_{St}} \tag{2}$$

Since the co-flow velocity has a strong relationship with the flame lift-off height (and hence soot formation, as seen in Section 3), it was calculated as the mean air co-flow velocity at the burner exit through the following equation:

$$V_{co-flow} = \frac{\dot{m}_{air}}{A \cdot \rho_{air}} \left[\frac{m}{s}\right] \tag{3}$$

where $\dot{m}_{air}$ is the air mass flow rate, A is the area of the cross-section of the burner exit, and ρ_{air} is the air density. Note these parameters were varied throughout this study (see Table 3), resulting in a wide range of velocities that covering from 7.5 to 20.5 ms^{-1}.

2.5. Droplet/spray estimate

Since the droplet size is an important parameter that significantly influences both flame lift-off height and soot formation (as will be seen in the following sections), its estimation through experimental correlations was first performed, allowing to notice the differences between tested fuels and the effect of increasing the fuel mass flow rate. The SMD has been calculated through three well-known correlations for pressure swirl atomizer: [37,71], and Lefebvre [43]:

$$SMD_{Radcliffe} = 7.3\sigma_l^{0.6}\nu_l^{0.2}\dot{m}_l^{0.25}\Delta P^{-0.4} \tag{4}$$

$$SMD_{Jasuja} = 4.4\sigma_l^{0.6}\nu_l^{0.16}\dot{m}_l^{0.22}\Delta P^{-0.43} \tag{5}$$

$$SMD_{Lefebvre} = 2.25\sigma_l^{0.25}\mu_l^{0.25}\dot{m}_l^{0.25}\Delta P^{-0.5}\rho_{air}^{-0.25} \tag{6}$$

where σ_l is the liquid surface tension, μ_l and ν_l are the dynamic and kinematic liquid viscosities, respectively; $\dot{m}_l$ is the liquid mass flow rate, ΔP is the pressure drop across the spray nozzle and ρ_{air} is the surrounding air density. All properties used in the SMD calculations are listed in Table 2. Since the fuel injection is in the ambient, the pressure drop is measured through a pressure sensor installed upstream from the nozzle.

Fig. 10, shows the SMD predicted according to Eqs. (4)–(6) for the fuels used in this work. These correlations have been widely used in both experimental [4,90] and computational [21] studies, and the predicted SMD followed the same trends between the different fuels observed in the measurements. The fuels show different droplet sizes at almost constant fuel mass flow rate: n-Dodecane exhibits the largest droplet sizes, followed by n-Decane and then n-Heptane. This variation is due to the differences in physical properties, particularly ones which are included in Eqs. (4)–(6) (density, surface tension, and viscosity). Amongst the fuels, viscosity is the property that varies more importantly. Since n-Dodecane has the highest viscosity (see Table 3), it exhibits the largest droplet size. Fig. 10 also shows the effect of modifying the fuel mass flow rate on SMD, evidencing that increasing $\dot{m}_l$ reduces the SMD. This fact can be directly related to the associated increasing injection pressure, which enhances the atomization quality.

3. Results and discussion

This section is divided into two parts, with the first subsection presenting the lift-off height measurements from OH* chemiluminescence images and the second one reporting the results of soot extinction in terms of K (i.e. after computing Abel inversion transform on the KL extinction images). The experiments were carried out for a range of co-flow conditions with a centrally mounted fuel spray nozzle. The effect of varying certain parameters such as co-flow velocity, fuel mass flow rate and preheated co-flow conditions on the flame lift-off height and soot formation were experimentally investigated.

3.1. Flame lift-off height

As was previously mentioned, the flame lift-off height is the point where the local flame propagation speed and the air-fuel mixture velocity are the same. This point can be affected by the interconnection of several processes such as atomization, vaporization, and chemical kinetics, which are in turn influenced by the operating conditions tested and fuel type. Therefore, the effects of varying these parameters on the flame lift-off height will be addressed throughout the current study. Note that flame lift-off heights in the following sections have a maximum relative standard deviation from the mean value equal to 2%.

3.1.1. Effect of fuel mass flow rate and air mass flow rate on the flame lift-off height

Fig. 11 shows the effect of varying the air mass flow rate (Fig. 11a) and fuel mass flow rate (Fig. 11b). Meanwhile, co-flow temperature and air outlet diameter were kept constant. Please note that Figs. 11 and 12 only show results for the n-Decane fuel, allowing to readily visualize the trends. The other two fuels follow the same trends presented here. Some observations from Fig. 11 can be made:

- In Fig. 11a, it is seen that the flame lift-off height has a direct relationship with the air mass flow rate, which is in turn related to the co-flow velocity calculated at the exit burner through Eq. (3) (for this case 9.8, 11.1 and 12.6 ms^{-1} for the air mass flow rates, i.e., 11.9, 13.6 and 15.6 kg h^{-1}, respectively). Various works [4,41,72] reported the same trend. Please note that the droplets move in a co-flow field with a resultant velocity (V_r), which is the resultant of droplet ejection velocity ($V_{droplet}$) and the air co-flow velocity ($V_{co-flow}$). Assuming both constant fuel mass flow rate (i.e., same injection pressure) and air co-flow temperature for a specific fuel, as the air co-flow velocity increases the resultant velocity of the mixture drives the droplets straight to a downstream position. Hence, so does the flame stabilization point (i.e., higher flame lift-off height). Additionally, Kumar et al. [41] introduced the effect of the air co-flow velocity on the computational estimation of the flame

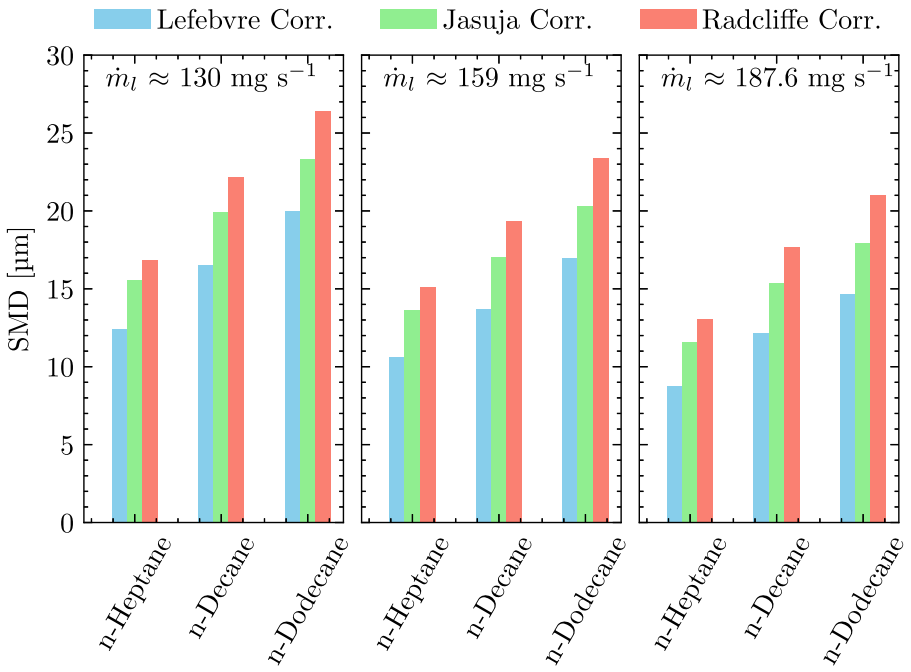

Fig. 10. Predicted SMDs for the tested fuels at air co-flow temperature of 328 K and air mass flow rate of 11.9 kg h^{-1}. The accurate fuel mass flow rates for each fuel are listed in Table 3.

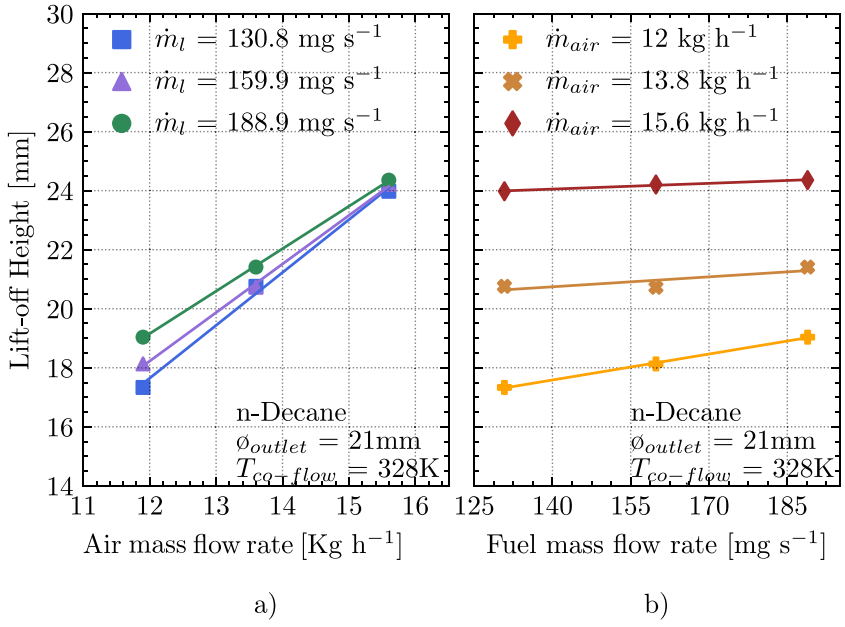

Fig. 11. Variation of the flame lift-off height with the air mass flow rate (a) and fuel mass flow rate (b), both for n-Decane fuel and a fixed air co-flow temperature.

lift-off height, finding that increasing this velocity leads to an increase in the chemical time scale, thus reducing the global reaction rate of the mixture. This leads to a reduction of the laminar flame speed (S_L) and hence an increase in the flame lift-off height.

- Fig. 11b shows the effect of increasing the fuel mass flow rate, which is done by increasing the injection pressure of the system. Please recall Section 2.5 that increasing the mass flow rate for a given fuel leads to a reduction in the SMD [5,64]. Thus, the droplet evaporation time is reduced, which should result in flame lift-off height reduction (this trend was reported by Reddy et al. [72], who used a similar injector type but with a bigger injector orifice diameter, lower injection pressures and also lower velocities of co-flow). However, the trends here shown do not follow this criterion. This fact is probably due to the fact that increasing the fuel mass flow rate at fixed air mass flow rate is known to result in an increase in the velocity of droplet ejection ($V_{droplet}$), thus increasing V_r [5] and therefore moving the stabilization point to a downstream position (i.e., higher flame lift-off height). Furthermore, it can be seen that this effect is almost negligible at high co-flow velocities (i.e., air mass flow rate of 15.6 kg h^{-1}), which control the V_r. Please note that the nozzle orifice diameter is small (see Section 2.1) and the injection pressures were relatively high (9.5, 15 and 21bar

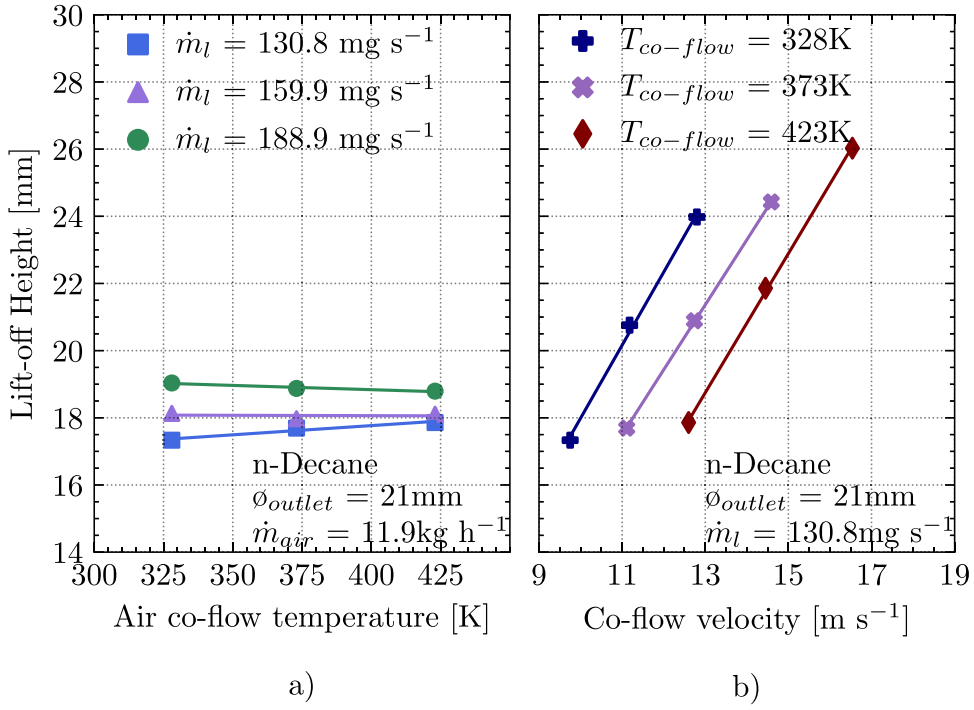

Fig. 12. Variation of the flame lift-off height with the air co-flow temperature (a) and co-flow velocity (b), both for n-Decane fuel.

for the fuel mass flow rates of 130.8, 159.8, and 190 mg s^{-1}, respectively).

3.1.2. Effect of the co-flow temperature on the flame lift-off height

Fig.12a shows the effect of varying the temperature of the air co-flow at fixed air mass flow rate (e.g., 11.9 kg h^{-1}). It is important to note that the observed trend is masked by the co-flow velocity: increasing the co-flow temperature reduces the air density, thus increasing the co-flow velocity (9.8, 11.1 and 12.6 ms^{-1} for the co-flow temperatures 328, 373, and 423K, respectively). In order to isolate the effect of the co-flow temperature on flame lift-off height, the Fig. 12b was introduced, where it can be seen that, for a constant air co-flow velocity, increasing the co-flow temperature significantly reduces the flame lift-off height. This fact evidences again that the stabilization position of the flame strongly depends on the fuel vapor/air mixture formation and its resultant velocity (V_r). The droplet vaporization rate is enhanced by the increase in the co-flow temperature, which purely depends on droplet number density and entrainment rate of hot co-flow [72]. Additionally, increasing the co-flow temperature increases S_L, which in turn affects the rate of the flame propagation through the spray. Myers and Lefebvre [54] derived a correlation to predict flame propagation through the quiescent multi-droplet mist, S_{spray}, taking into account the evaporation rates and chemical reaction rates (related to S_L). As the laminar flame speed increases, S_{spray} also increases, causing stabilization of the flame closer to the injector tip (i.e., lower flame lift-off height)[4].

3.1.3. Effect of fuel type on the flame lift-off height

Since previous subsections have not yet shown the effect of the fuel type on the flame lift-off height, this subsection has been introduced. In Fig. 13, flame lift-off height is plotted against air mass flow rate for the three co-flow temperatures tested. From the results, it is possible to observe some trends previously discussed, such as the air mass flow rate influence, but the purpose here is to remark the effect of fuel type on the flame lift-off length.

In general, larger droplet sizes and less volatile fuels exhibit higher lift-off heights as depicted in Fig. 13. For instance, this is seen for a fixed nozzle size in the n-Dodecane fuel (the volatility of the fuel is represented by the fuel vapor pressure in Table 2 and it was described in Section 2.5, the droplet size depending on fuel properties such as density, viscosity and surface tension). This is due to n-Dodecane needing more time/length to evaporate and generate enough vapor to stabilize the flame against the incoming reactant stream. n-Heptane exhibits a lower lift-off height, which can be attributed to its higher volatility and its smaller droplet size, which enhances the fuel/air mixing, resulting in a higher fraction of localized pre-mixed fuel-lean regions [73,74]. The same behavior was noticed in a related work [4]. Since the n-Decane presents intermediate values of both volatility and droplet size, it is expected for n-Decane to present intermediate lift-off heights, as shown in Fig. 13.

3.1.4. Air outlet diameter effect on the flame lift-off height

The effect of replacing the air outlet diameter on flame lift-off height is shown in Fig. 14 for the three fuels and the three air mass flow rates tested under fixed conditions of fuel mass flow ratre and air co-flow temperature. Fig. 14 also shows fit lines for each outlet diameter. In order to examine the effect that the air outlet diameter over the lift-off height, the co-flow velocity must remain constant. For every fuel shown in Fig. 14 and a fixed co-flow velocity, the flame lift-off height increases as the outlet cross-section is increased (i.e., air outlet diameter). The difference between these points is the global equivalence ratio, which in the case of the air outlet diameter of 21 mm is considerably leaner than for the 19 mm one. This reduction is attributed to the increase in the air mass flow rate needed to achieve the same co-flow velocity. Myers and Lefebvre [54] reported that flame speed (S_{spray}) increases with the overall equivalence ratio up to the stoichiometric value for a wide range of fuels and test conditions. Consequently, as the flame speed increases, the flame lift-off height decreases [4]. Myers and Lefebvre [54] also observed that for heavier fuels, the flame speed is more sensitive to the fuel/air ratio.

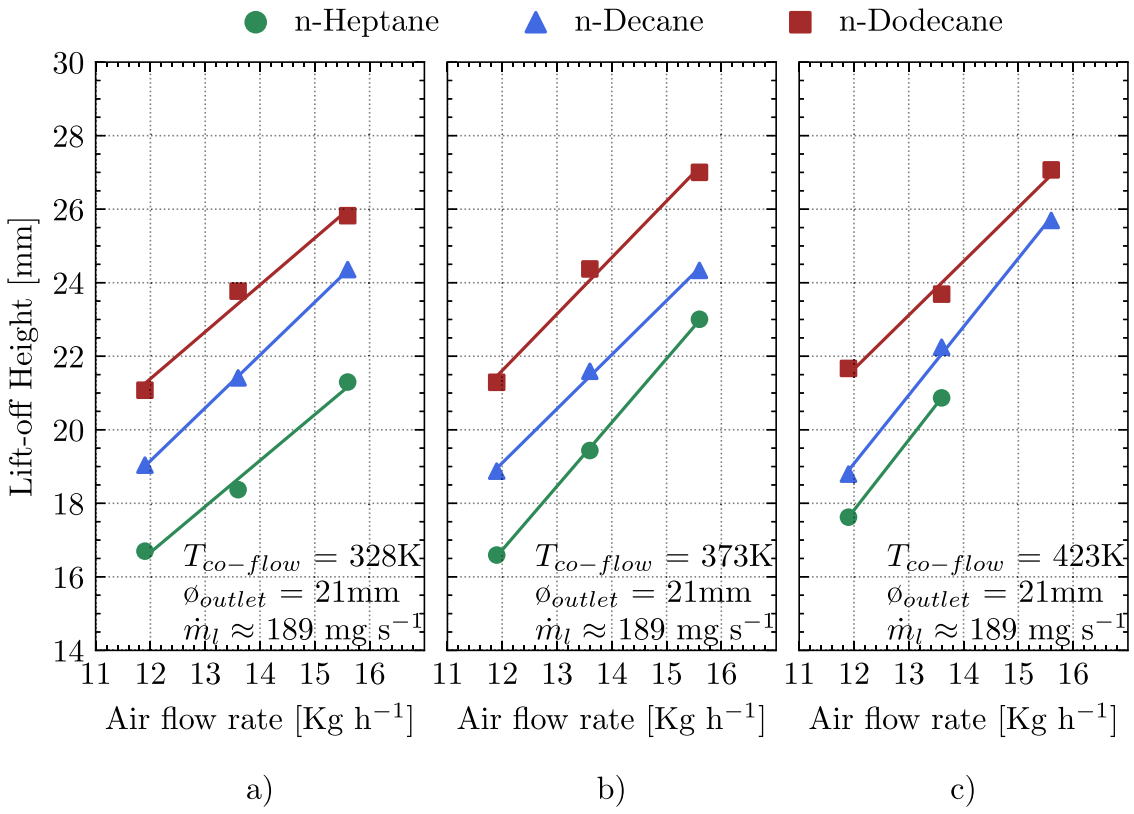

Fig. 13. Flame lift-off heights against the air mass flow rate for the different fuels, at co-flow temperatures of 328K (a), 373K (b), and 423K (c) at constant fuel mass flow rate (accurate values for each fuel are listed in Table 3). Symbols correspond to the fuel type and fit lines were plotted for each fuel.

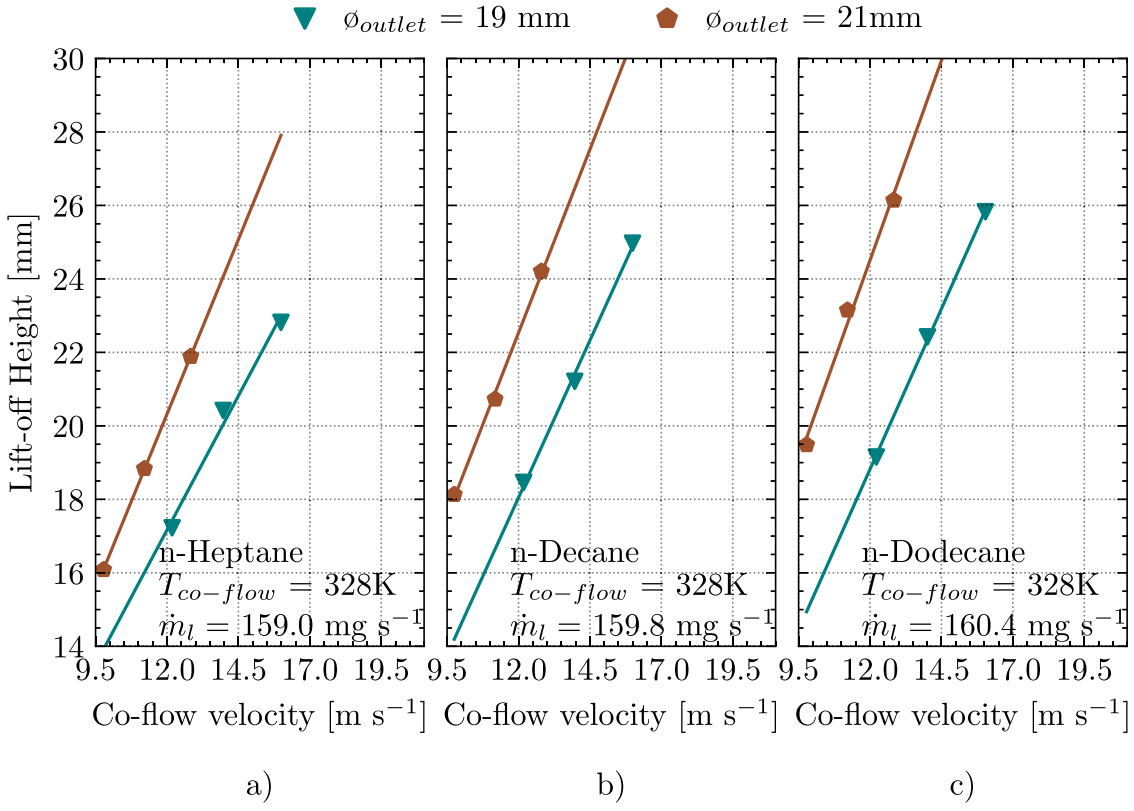

Fig. 14. Flame lift-off heights against the co-flow velocity for the different fuels, n-Heptane (a), n-Decane (b), and n-Dodecane (c) at constant fuel mass flow rate and co-flow temperature.

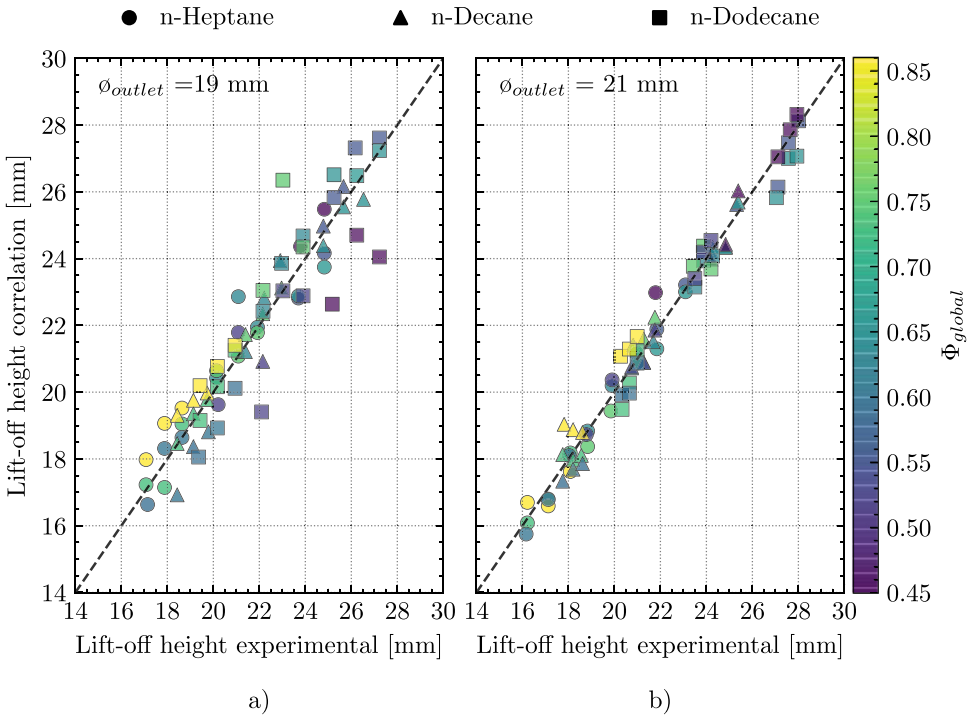

Fig. 15. Comparison between experimental results and the correlation ones for the air outlet diameters of 19 mm (a) and 21 mm (b), all fuels, and all operating conditions.

3.1.5. Statistical analysis

The wide range of operating conditions tested allows performing a statistical analysis. Empirical correlations have been used by many researchers as an attempt to explain the effect of varying the surrounding conditions, injection pressure, and fuel type on the flame lift-off height [6,65,69,72]. From the results presented earlier, it can be assumed that the flame lift-off height is probably controlled by the air co-flow velocity, fuel type (droplet size and volatility), co-flow temperature and also the global equivalence ratio. Reddy et al. [72] studied the effect of these parameters on the lift-off height, reporting that the lift-off height is a strong function of co-flow velocity and Sauter mean diameter, although in the present work the droplet size was not measured. The statistical analysis was performed individually for each fuel and each air outlet diameter. With the rest of the parameters, the outcomes showed that only air co-flow velocity and co-flow temperature are significant in the flame lift-off height estimation as presented in Eq. (7):

$$LOH \propto T_{co-flow}^{a} \cdot V_{co-flow}^{b} \tag{7}$$

where LOH [mm] corresponds to the flame lift-off height, $T_{co-flow}$ [K] to air co-flow temperature, and $V_{co-flow}$ [ms^{-1}] corresponds to mean air co-flow velocity at the burner exit. Eq. (7) seems to be reasonable due to the fact that the droplet evaporation time is a function of the air temperature, droplet diameter and air entrainment, which in turn depends on co-flow velocity. Therefore, the variation of the coefficients between fuels (Table 4), is likelly related to fuel volatility and reactivity on the one hand; and to droplet size (which is a direct function of all liquid properties, i.e. surface tension, density and viscosity), mass flow rate and the injection presure on the other hand. Table 4 summarizes the results from Eq. (7) for each fuel and both air outlet diameters. The flame lift-off height varies linearly with the air velocity, whereas the air temperature has an inverse effect as expected by the findings mentioned earlier. In any case, the values of R^2 confirm the good repeatability and reliability of the results gathered. There is, relatively less reliability for the air outlet diameter of 19 mm, as seen in Fig. 15. This is because a significant number of operating conditions promote the flame blow-off phenomenon for the air outlet diameter of 19 mm. This phenomenon occurs if the fuel vapor-air mixture is too lean to burn and the co-flow velocity is too high to stabilize the flame and was principally observed for n-Heptane due to its high volatility and the increase in co-flow velocity.

Table 4
Empirical correlation results for lift-off height.

Fuel	Air outlet diameter	a	b	R^2
n-Heptane	19 mm	-0.874	1.205	0.94
	21 mm	-0.67	1.0977	0.97
n-Decane	19 mm	-0.82	1.09	0.95
	21 mm	-0.963	1.14	0.98
n-Dodecane	19 mm	-0.655	0.953	0.8
	21 mm	-0.9307	1.06	0.96

3.2. Soot formation

In order to help understanding the influence of the parametric variations on soot formation, the current section presents four subsections: first, the effect of the operating conditions, followed by the fuel type effect; then the influence of the air outlet diameter; and finally, a summary of all tested conditions. The results presented throughout this section are the result of processing the images captured by the diffused back-illumination extinction technique and following the methodology previously detailed. Furthermore, the results are presented in terms of the measured light attenuation by the soot cloud in a horizontal sheet-of-sight perspective (KA) and the total amount of soot (KV), as presented in Fig. 16.

Soot originates from the incomplete combustion of hydrocarbons fuels, indicating in most cases poor combustion conditions, where not all the fuel can be completely oxidized. Experimental results from different studies of liquid fuel spray combustion

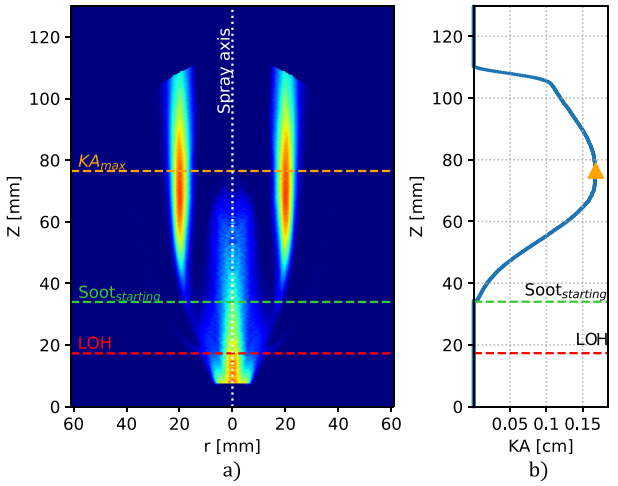

Fig. 16. (a) Light attenuation by the soot cloud in terms of K, (b) *KA* evolution profile through the flame height. The frame shown is a n-Decane flame with an air co-flow temperature of 328 K, for an air mass flow of 11.9 kg h^{-1} and fuel mass flow of 131 mg s^{-1}.

have shown the effect of operating conditions and fuel type on soot formation [19,88,93,94]. Unfortunately, as described [88] soot formation during the burning of fuel sprays depends not only on soot chemistry but on many other physical processes such as spray penetration, droplet size distribution, and velocity field of the entrained air. Therefore, it is challenging to isolate these factors to obtain quantitative information on soot behaviors. Some relationships have been observed between the operating conditions and soot formation, one of them being the strong relationship between the lift-off height and soot formation [63,68,69]. For a particular fuel, as the lift-off height increases, the air entrainment increases, providing a less-rich reaction zone just downstream of the flame lift-off height, thus resulting in less soot formation.

3.2.1. Effect of co-flow conditions and fuel mass flow rate on soot formation

Fig. 17 shows the effect of varying the air co-flow temperature, air mass flow rate (co-flow velocity),and fuel mass flow rate on soot formation for a given air outlet diameter (21 mm) and fuel (n-Decane). Some observations from Fig. 17 can be made:

- Air co-flow velocity seems to be the parameter driving soot formation. As the air co-flow velocity increases, the flame stabilizes further away from the injector tip (Fig. 17a), i.e., the amount of air entrainment increases. Thus there are less-rich conditions at the reaction zone just downstream of the flame lift-off height, which results in less soot formation due to the major availability of O_2 to oxidize the fuel molecules. It can be observed that as co-flow velocity decreases, the location of the maximum *KA* value is moved further downstream. A reduction in the co-flow velocity results in a longer flame length with a larger yellow-sooting diffusion region and a smaller blue region (partially premixed), moving the location of the maximum *KA*. The location of the maximum *KA* is also affected by varying the fuel mass flow rate, as shown in Fig. 17.
- The effect of the co-flow temperature observed here is almost negligible for a constant velocity. Soot formation is a process highly sensitive to temperature [88]. Also, an increase in the co-flow temperature increases the evaporation rate, which in turn reduces the flame lift-off height (see Fig. 17a). Thus, it reduces the amount of air entrainment, leading to an establishment of a rich primary zone likely contributing to the soot formation. However, this enhancement of the droplet evaporation rate also leads to a reduction of the droplet size and hence the number of droplets that reach the yellow-sooting diffusion flame is lower thus reducing soot formation. Hayashi et al. [32] conducted a detailed experimental and numerical investigation for a n-Decane spray flame in a laminar counterflow field, reporting that as the initial droplet size increased, an initially blue reaction zone transitioned towards yellow flames with increasingly higher luminosity, showing an enhancement of both the peak of soot concentration and the sooting zone area. The two previous facts lead to conclude that during the experiments the effect of the droplet size is higher than the effect of air entrainment, resulting in a balance of both effects. On the contrary, some authors reported [26,63,95] that increasing the temperature of the surrounding air also increases the amount of soot, attributing this effect to a reduction of the amount of air entrainment. This suggests that their experiments present a "droplet-driven" flame lift-off height, whereas the present work could be "co-flow driven" (see Fig. 11b), considering that the other works were conducted at relatively low co-flow velocities.
- Fig. 17 also shows the effect of varying the fuel mass flow rate. For a constant co-flow velocity, increasing the fuel mass flow rate significantly increases soot formation. As the fuel mass rate increases the equivalence ratio increases, i.e., rich conditions at the reaction zone just downstream of the flame lift-off height, enhancing the soot formation.

3.2.2. Effect of fuel type on soot formation

Fig. 18 presents the evolution of *KA* along the flame height for different operating conditions and the three fuels tested. Fig. 18 shows that the number of operating conditions that promote the soot formation is higher for n-Decane and n-Dodecane than for n-Heptane fuel and that soot formation increases by increasing the global equivalence ratio (i.e., lower air mass flow rate and higher fuel mass flow rate). In Fig. 18, comparing the yellow markers (i.e., same global equivalence ratio and same co-flow velocity) for n-Decane and n-Dodecane it becomes evident that the soot formation is larger for n-Dodecane. In order to observe the effect of the fuel type on soot formation at a constant co-flow velocity, Fig. 19 was introduced, where *KV* is plotted against the co-flow velocity for the three fuels. From Fig. 19, it is again clear that n-Dodecane fuel has a higher sooting tendency, followed by n-Decane and then distantly by n-Heptane, exhibiting for this set of results a slight soot formation only at the lowest co-flow temperature and non-perceptible for the other two co-flow temperatures. As several authors have mentioned, it is natural to suspect that certain fuels are inherently more sooting than others, which is generally accepted since the fuel molecular structure is critical in determining the sooting tendencies of a combustion system [28,57,88]. In order to assess the sooting tendencies, different sooting indexes have been developed. Calcote and Manos [10] introduced the threshold soot index (TSI), where higher values mean higher sooting propensity and [51] introduced the yield sooting index (YSI). Olson et al. [57] provided a set of diffusion flame soot threshold data, including both TSIs values and maximum soot volume fraction, f_v(max), for 103 pure hydrocarbons. From this data, it is found that the fuel with higher values of both f_v(max) and TSI is n-Dodecane fuel, followed closely by n-Decane and then n-Heptane with a considerable difference (see Table 5). Olson et al. [57] also mentioned that, for alkane fuels (e.g., n-Heptane, n-Decane and n-Dodecane) the sooting tendency generally increases in a slight manner with an increase in the number of carbon chains in the molecule. In Fig. 19, it may be seen that soot formation follows the statement previously mentioned among the fuels, evidencing the strong dependence of soot formation on the fuel sooting tendency.

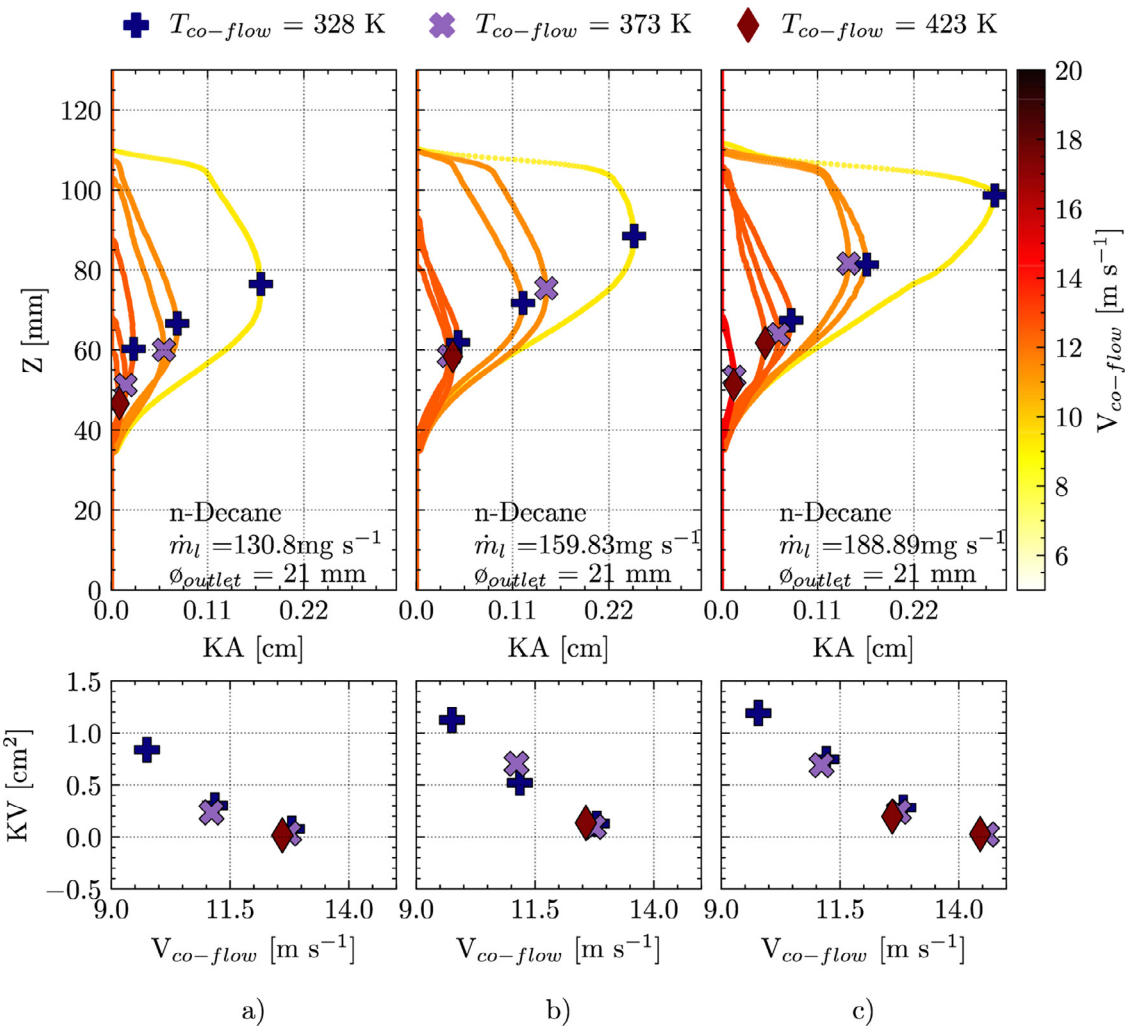

Fig. 17. Light attenuation by the soot cloud, in terms of *KA* and *KV*, for n-Decane fuel at fuel mass flow rates of 130.8 mg s^{-1} (a), 159.53 mg s^{-1} (b) and 188.89 mg s^{-1} (c). Top images show the *KA* evolution throughout the flame height and its maximum value, which is pointed out by the location of the symbols. Symbols are in turn related to the co-flow temperature. Bottom images show the total soot, *KV*, against the co-flow velocity.

Table 5
Sooting tendency values measured by Olson et al. [57] for diffusion flames.

Properties	n-Heptane	n-Decane	n-Dodecane
Threshold soot index (TSI)	2.0	3.9	5.4
$f_v(max)$ (10^{-6})	2.0	3.4	3.5

3.2.3. Air outlet diameter effect on soot formation

The effect of varying the air outlet diameter on soot formation for n-Decane and n-Dodecane fuels at fixed conditions of fuel mass fuel rate and co-flow temperature is presented in Fig. 20. For a constant velocity, it can be seen that soot formation increases with a reduction of the outlet cross-section (i.e., air outlet diameter). As was explained previously, a reduction in the air outlet diameter causes a reduction of the flame lift-off height (see Fig. 14), hence, the amount of air entrainment is reduced (i.e., a reduction of the availability of the of O_2) to oxidize the fuel molecules, which results in increasing the amount of soot.

3.2.4. Summary

Figures from the previous subsections only show partial sets of results. Hence, Fig. 21 is introduced as a summary to present all the tested conditions that promote the soot formations. In Fig. 21, *KV* is plotted against the co-flow velocity, which is divided by fuel type and air outlet diameter. The vertical axis was set on a logarithmic scale due to the large differences in the soot concentration between fuels. Fig. 21 shows some of the previously described facts, such as the large influence of the co-flow velocity on soot formation for every fuel. An inverse behaviour is exhibited: as the co-flow velocity increases the soot formation is reduced. The previous fact is likely due to co-flow velocity playing a significant role in the flame lift-off height limits, and therefore on the amount of air entrainment, which delimits the availability of O_2 to oxidize the fuel molecules. Furthermore, another clear fact is the dependence of the soot formation with the fuel sooting tendency, showing a large formation for n-Dodecane fuel, followed closely by n-Decane, and finally with a notorious difference n-Heptane. Finally, the fuel mass flow rates and co-flow temperature do not exhibit a notorious effect linked to the commented co-flow velocity and fuel mass flow rate effects.

4. Conclusions

In the present work, the effect of co-flow conditions and fuel mass flow rate are tested for different fuels (n-Heptane, n-Decane, and n-Dodecane), which present significant differences in physical properties that impact the atomization process. The flame lift-off height and soot formation have been experimentally investigated

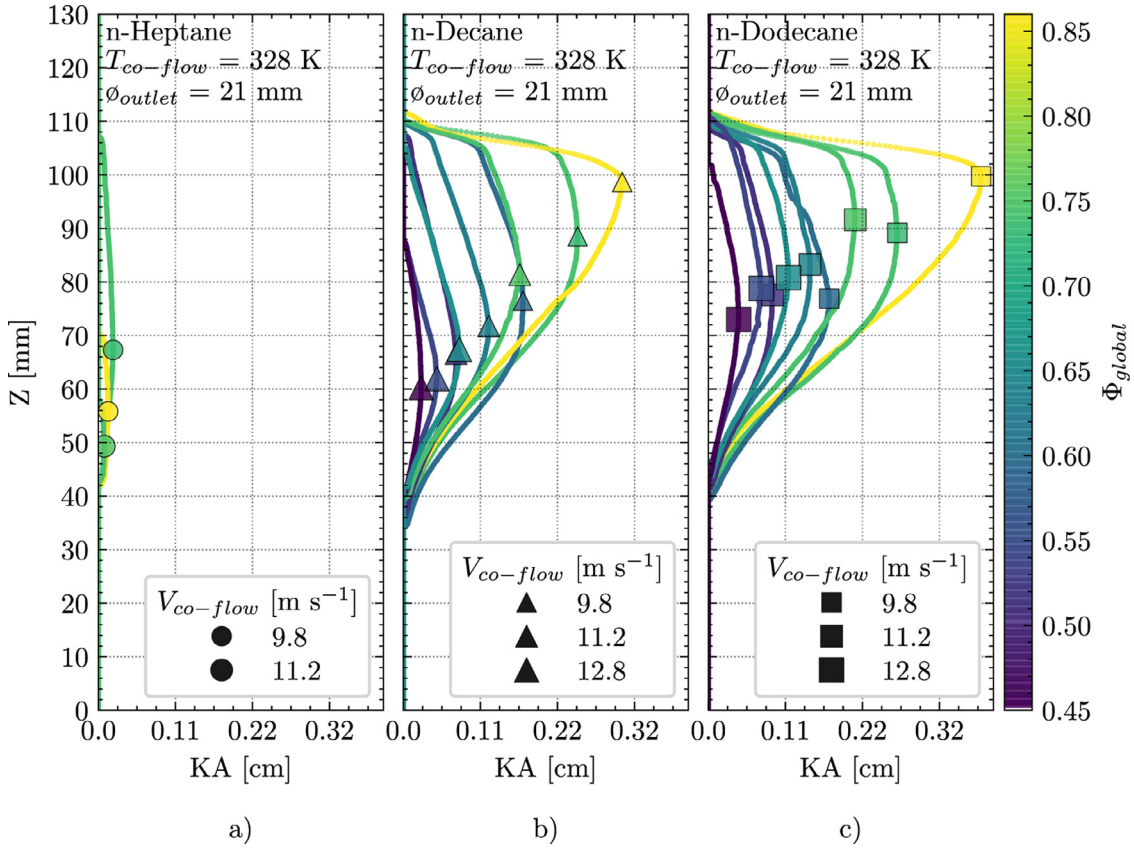

Fig. 18. *KA* evolution throughout the flame height for the different fuels, n-Heptane (a), n-Decane (b), and n-Dodecane (c), at a fixed air temperature of 328K and air outlet diameter of 21 mm. Lines and symbols are colored by the global equivalence ratio and the size of the marker is related to co-flow velocity.

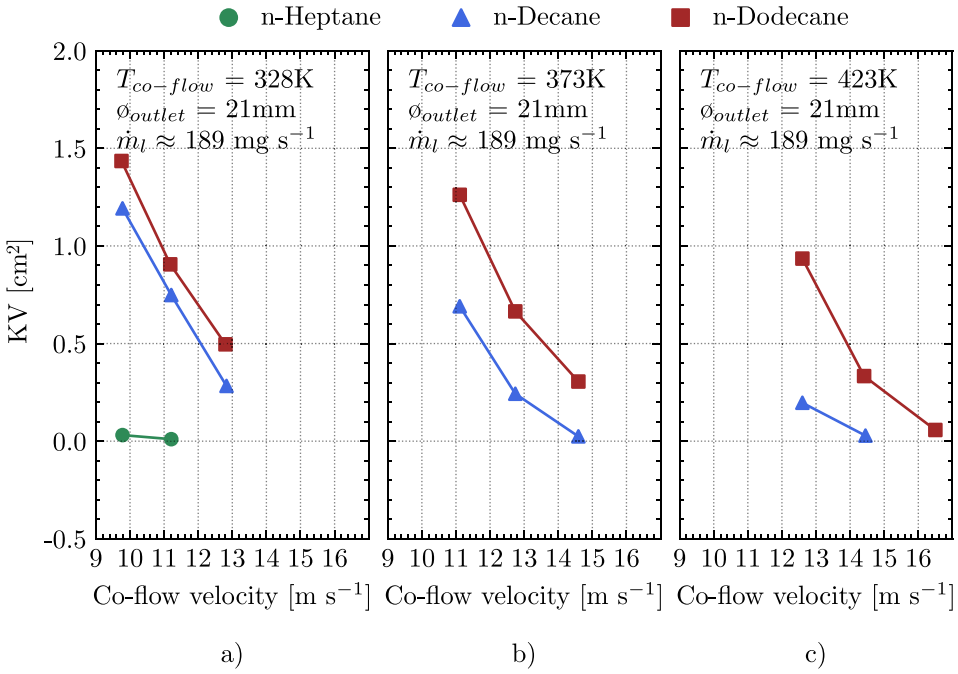

Fig. 19. *KV* against air mass flow rate at different co-flow temperatures of 328 (a), 373 (b) and 423 K (c) and air outlet diameter of 21 mm (accurate values of fuel mass flow rate for each fuel are listed in Table 3).

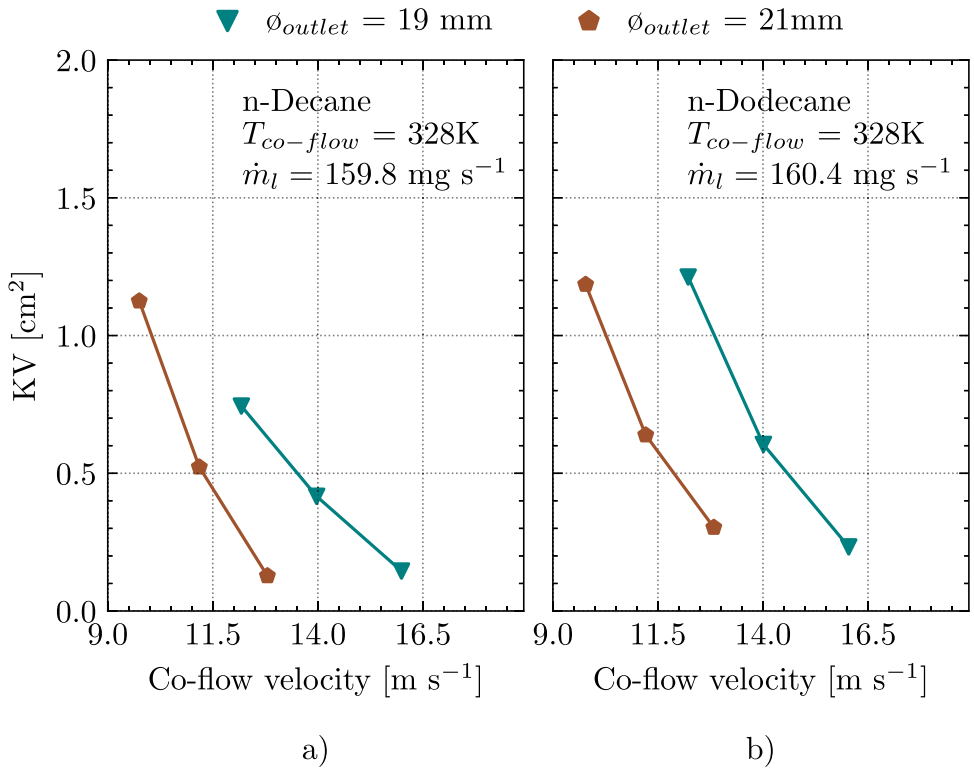

Fig. 20. Effect of air outlet diameter on soot formation, at fixed conditions of co-flow temperature of 328K and fuel mas flow rate of 160 mg s^{-1} for n-Decane (a) and n-Dodecane (b) fuels.

through the OH* chemiluminescence and diffuse back-illumination extinction techniques, respectively. Fuels were injected through a hollow cone spray injector in a preheated air co-flow. From the findings, it is possible to conclude that:

- For a particular fuel, the flame lift-off height is largely controlled by the co-flow velocity. As co-flow velocity increases, the resultant velocity drives the droplets straight to a downstream position and thus moving the stabilization point of the flame.
- Isolating the effect of the co-flow temperature, it has been observed that flame lift-off height varies inversely with increases in co-flow temperature. The reason is that an increase in the air temperature leads to an increase in the fuel vaporization rate, which results in a reduction in the flame lift-off height.
- The influence of the fuel type on the flame lift-off height seems to be related to both fuel volatility and droplet size, which depend on the fuel physical properties such as density, viscosity, and surface tension. The larger the droplet size and the lower the fuel volatility (e.g., n-Dodecane) the higher the measured lift-off height. As a result, this increases the time necessary to evaporate the fuel droplets and generate enough vapor to stabilize the flame against the incoming reactant stream.
- Isolating the effect of the air outlet diameter, it has been observed that as the air outlet diameter increases, the flame lift-off height is increased. This behavior is attributed to a lower global equivalence ratio, which causes a reduction in the flame speed.
- The statistical analysis performed for each fuel and each outlet diameter evidences the strong dependence of flame lift-off height with the co-flow velocity and co-flow temperature, which affect the resultant velocity of the mixture and evaporation rates, respectively.
- Soot formation is significantly controlled by the co-flow velocity. As the co-flow velocity increases, the droplets are quickly transported further away from the injector tip, increasing the amount of air entrainment. Thus, a lean mixture is formed further downstream, which results in a less soot formation.
- Isolating the co-flow temperature effect on soot formation it was observed that its influence is almost negligible. This is likely due to the balance of two effects: on the one hand, increasing the co-flow temperature enhances the evaporation rates, which reduces the flame lift-off length (i.e., a reduction of the amount of air entrainment), establishing a rich primary zone that enhances the soot formation. On the other hand, the co-flow temperature leads to a reduction of the droplet size and hence the number of droplets that reach the yellow-sooting region of the flame, resulting in a reduction in the soot formation.
- Isolating the effect of the air outlet diameter on the soot formation, it was observed that reducing the air outlet diameter enhances soot formation. This is likely due to the reduction in the amount of air entrainment before the reaction zone, which promotes a rich reaction zone.
- The trends observed from the experimental results exhibit that soot formation is a complex process that is affected by several parameters such as the amount of air entrainment, fuel evaporation rate, the global equivalence ratio, and mainly the sooting tendency of the fuel since they control the conditions in the reaction zone just downstream of the flame lift-off height.

Declaration of Competing Interest

The authors declare that they have no known competing financial interests or personal relationships that could have appeared to influence the work reported in this paper.

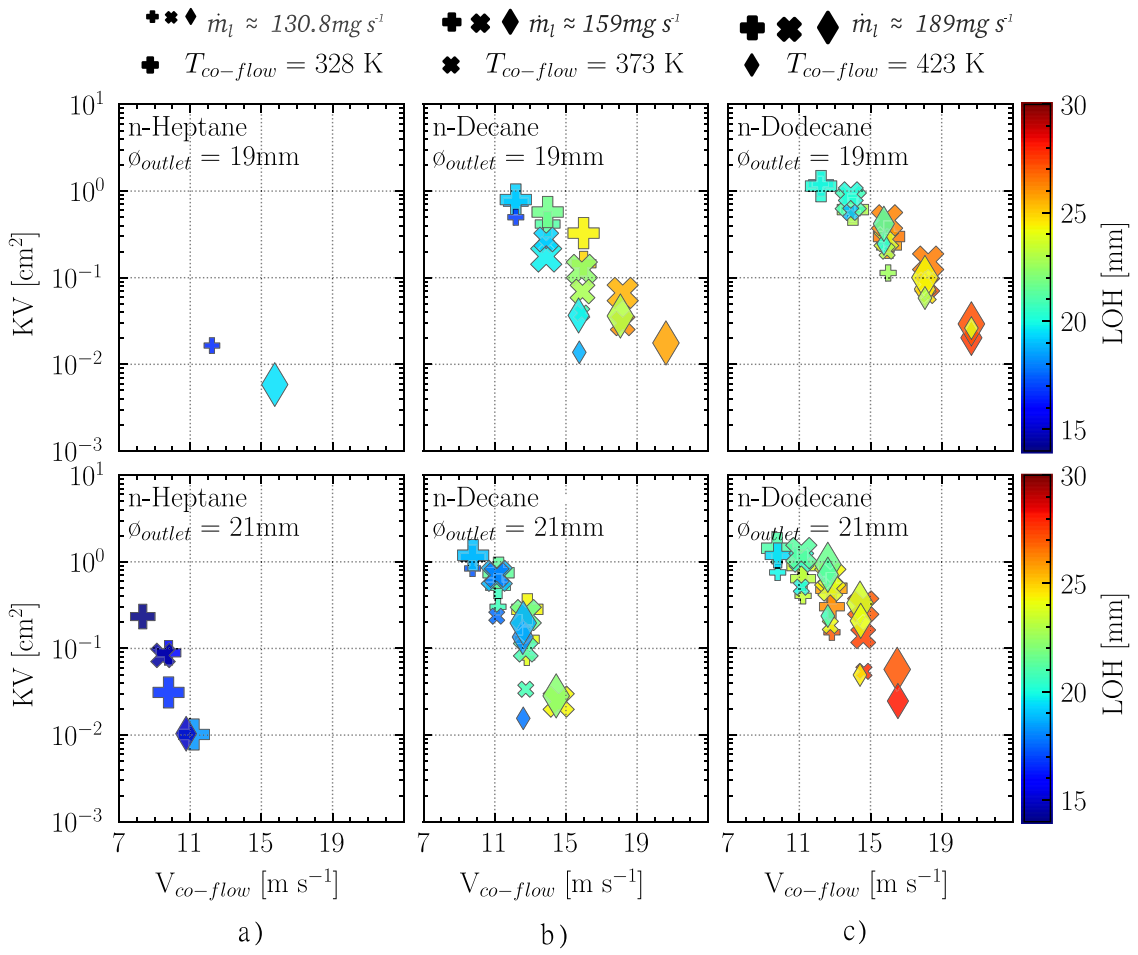

Fig. 21. Relationship between flame lift-off height and total light attenuation by soot concentration (*KV*), for all operating conditions and the different fuels: n-Heptane (a), n-Decane (b) and n-Dodecane (c) (accurate values of fuel mass flow rate for each fuel are listed in Table 3). Symbols represent the co-flow temperature and its size the fuel mass flow rate, and also colored by the flame lift-off height.

Acknowledgments

This research was funded bythe Spanish Ministerio de Ciencias, Investigación y Universidades through project RTI2018-099706-B-I00. Part of the experimental hardware was purchased through funds obtained from Spanish Ministerio de Ciencias, Investigación y Universidades and FEDER through project EQC2019-005818-P. The author Santiago Cardona Vargas would like to thank Universitat Politécnica de Valéncia for his Predoctoral contract (FPI-2016-S1), which is included within the framework of Programa de Apoyo para la Investigación y Desarrollo (PAID-01-2016). The authors are thankful to Jose Enrique Del Rey and Omar Huerta for helping in the technical issues, also to Carlos Gil Martínez for helping during the experimental campaign.

References

[1] F. Akamatsu, Y. Miutani, M. Katsuki, S. Tsushima, Y.D. Cho, Measurement of the local group combustion number of droplet clusters in a premixed spray stream, Symp. (Int.) Combust. 26 (1996) 1723–1729, doi:10.1016/S0082-0784(96)80397-3.

[2] Y.M. Al-Abdeli, A.R. Masri, Review of laboratory swirl burners and experiments for model validation, Exp. Therm. Fluid Sci. 69 (2015) 178–196, doi:10.1016/j.expthermflusci.2015.07.023.

[3] M.G. Allen, K.R. McManus, D.M. Sonnenfroh, P.H. Paul, Planar laser-induced-fluorescence imaging measurements of OH and hydrocarbon fuel fragments in high-pressure spray-flame combustion, Appl. Opt. 34 (27) (1995) 6287, doi:10.1364/ao.34.006287.

[4] R. Alsulami, B. Windell, S. Nates, W. Wang, S.H. Won, B. Windom, Investigating the role of atomization on flame stability of liquid fuels in an annular spray burner, Fuel 265 (2020), doi:10.1016/j.fuel.2019.116945.

[5] R.A. Alsulami, S. Nates, W. Wang, S.H. Won, B. Windom, Effects of varying liquid fuel and air co-flow rates on spray characterisation of an annular co-flow spray burner, Proceedings of the ASME Turbo Expo, 4B-2019, American Society of Mechanical Engineers (ASME) (2019), doi:10.1115/GT2019-90989.

[6] J. Benajes, R. Payri, M. Bardi, P. Martí-aldaraví, Experimental characterization of diesel ignition and lift-off length using a single-hole ECN injector, Appl. Therm. Eng. 58 (1–2) (2013) 554–563, doi:10.1016/j.applthermaleng.2013.04.044.

[7] T.L. Berry, W.L. Roberts, Measurement of smoke point in velocity-matched coflow laminar diffusion flames with pure fuels at elevated pressures, Combust. Flame 145 (3) (2006) 571–578, doi:10.1016/j.combustflame.2005.12.010.

[8] J.A. Bossard, R.E. Peck, Droplet size distribution effects in spray combustion, Symp. (Int.) Combust. 26 (1996) 1671–1677, doi:10.1016/S0082-0784(96)80391-2. Elsevier

[9] G. Cabot, D. Vauchelles, B. Taupin, A. Boukhalfa, Experimental study of lean premixed turbulent combustion in a scale gas turbine chamber, Exp. Therm. Fluid Sci. 28 (7) (2004) 683–690, doi:10.1016/j.expthermflusci.2003.12.001.

[10] H.F. Calcote, D.M. Manos, Effect of molecular structure on incipient soot formation, Combust. Flame 49 (1–3) (1983) 289–304, doi:10.1016/0010-2180(83)90172-4.

[11] F. Carbone, A. Gomez, The structure of toluene-doped counterflow gaseous diffusion flames, Combust. Flame 159 (10) (2012) 3040–3055, doi:10.1016/j.combustflame.2012.05.003.

[12] A. Cessou, Simple description of the combustion structures in the stabilization stage of a spray jet flame, At. Sprays 9 (1) (1999) 1–27, doi:10.1615/AtomizSpr.v9.i1.10.

[13] T.T. Charalampopoulos, Morphology and dynamics of agglomerated particulates in combustion systems using light scattering techniques, 1992, 10.1016/0360-1285(92)90031-U

[14] S. Chatterjee, Ö.L. Gülder, Soot concentration and primary particle size in swirl-stabilized non-premixed turbulent flames of ethylene and air, Exp. Therm. Fluid Sci. 95 (2018) 73–80, doi:10.1016/j.expthermflusci.2018.01.035.

[15] H.H. Chiu, H.Y. Kim, E.J. Croke, Internal group combustion of liquid droplets, Symp. (Int.) Combust. 19 (1982) 971–980, doi:10.1016/S0082-0784(82)80273-7. Elsevier

[16] H.H. Chiu, C.L. Lin, Anomalous group combustion of premixed clusters, Symp. (Int.) Combust. 26 (1996) 1653–1661, doi:10.1016/S0082-0784(96)80389-4. Elsevier

[17] S.K. Choi, B.C. Choi, S.M. Lee, J.H. Choi, The effect of liquid fuel doping on PAH and soot formation in counterflow ethylene diffusion flames, Exp. Therm. Fluid Sci. 60 (2015) 123–131, doi:10.1016/j.expthermflusci.2014.08.008.

[18] F. Cignoli, S. De Iuliis, V. Manta, G. Zizak, Two-dimensional two-wavelength emission technique for soot diagnostics, Appl. Opt. 40 (30) (2001) 5370, doi:10.1364/ao.40.005370.

[19] S. De Iuliis, M. Barbini, S. Benecchi, F. Cignoli, G. Zizak, Determination of the soot volume fraction in an ethylene diffusion flame by multiwavelength analysis of soot radiation, Combust. Flame 115 (1–2) (1998) 253–261, doi:10.1016/S0010-2180(97)00357-X.

[20] M. Derudi, A. Villani, R. Rota, Sustainability of mild combustion of hydrogen-containing hybrid fuels, Proc. Combust. Inst. 31 (2) (2007) 3393–3400, doi:10.1016/j.proci.2006.08.107.

[21] P.S.B. Dikshit, D.D.B. Kulshreshtha, D.S.A. Channiwala, Numerical analysis and empirical correlations to predict SMD of pressure swirl atomizer for small scale gas turbine combustion chamber, Int. J. Appl. Eng. Res. 13 (2018) 4531–4537.

[22] A.J. Donkerbroek, M.D. Boot, C.C. Luijten, N.J. Dam, J.J. ter Meulen, Flame lift-off length and soot production of oxygenated fuels in relation with ignition delay in a DI heavy-duty diesel engine, Combust. Flame 158 (3) (2011) 525–538, doi:10.1016/j.combustflame.2010.10.003.

[23] B. Duret, G. Luret, J. Reveillon, T. Menard, A. Berlemont, F.X. Demoulin, DNS Analysis of turbulent mixing in two-phase flows, Int. J. Multiphase Flow 40 (2012) 93–105, doi:10.1016/j.ijmultiphaseflow.2011.11.014.

[24] I. Düwel, H.W. Ge, H. Kronemayer, R. Dibble, E. Gutheil, C. Schulz, J. Wolfrum, Experimental and numerical characterization of a turbulent spray flame, Proc. Combust. Inst. 31 (2) (2007) 2247–2255, doi:10.1016/j.proci.2006.07.111.

[25] M. Frenklach, H. Wang, Detailed modeling of soot particle nucleation and growth, Symp. (Int.) Combust. 23 (1) (1991) 1559–1566, doi:10.1016/S0082-0784(06)80426-1.

[26] A. Ghasemi, M. Moghiman, S.M. Javadi, N. Hosseini, Effects of droplet size and air preheating on soot formation in turbulent combustion of liquid fuel, ASME 2010 10th Biennial Conference on Engineering Systems Design and Analysis, ESDA2010, 1 (2010), pp. 211–217, doi:10.1115/ESDA2010-24663.

[27] J. Glasser, J. Chapelle, J.C. Boettner, Abel inversion applied to plasma spectroscopy: a new interactive method, Appl. Opt. 17 (23) (1978) 3750, doi:10.1364/ao.17.003750.

[28] I. Glassman, P. Yaccarino, The temperature effect in sooting diffusion flames, Symp. (Int.) Combust. 18 (1) (1981) 1175–1183, doi:10.1016/S0082-0784(81)80122-1.

[29] A.H.A. Hamid, R. Atan, Spray characteristics of jet-swirl nozzles for thrust chamber injector, Aerosp. Sci. Technol. 13 (4–5) (2009) 192–196, doi:10.1016/j.ast.2008.10.003.

[30] J. Hayashi, K. Terashima, F. Akamatsu, N. Tokuoka, Effect of the Drop Size Distribution of Fuel Spray on Ignition Phenomenon, Transactions of the Japan Society of Mechanical Engineers Series B, 74 (2008), pp. 1161–1168, doi:10.1299/kikaib.74.1161.

[31] J. Hayashi, H. Watanabe, R. Kurose, F. Akamatsu, Effects of fuel droplet size on soot formation in spray flames formed in a laminar counterflow, Combust. Flame 158 (12) (2011) 2559–2568, doi:10.1016/j.combustflame.2011.05.015.

[32] J. Hayashi, H. Watanabe, R. Kurose, F. Akamatsu, Effects of fuel droplet size on soot formation in spray flames formed in a laminar counterflow, Combust. Flame 158 (12) (2011) 2559–2568, doi:10.1016/j.combustflame.2011.05.015.

[33] D.D. Hickstein, S.T. Gibson, R. Yurchak, D.D. Das, M. Ryazanov, A direct comparison of high-speed methods for the numerical abel transform, Rev. Sci. Instrum. 90 (6) (2019) 065115, doi:10.1063/1.5092635.

[34] B. Higgins, D.L. Siebers, Measurement of the flame lift-Off location on DI diesel sprays using OH chemiluminescence, SAE Technical Paper (2001).

[35] L. Hu, Q. Wang, M. Delichatsios, S. Lu, F. Tang, Flame radiation fraction behaviors of sooty buoyant turbulent jet diffusion flames in reduced and normal atmospheric pressures and a global correlation with reynolds number, Fuel 116 (2014) 781–786, doi:10.1016/j.fuel.2013.08.059.

[36] J. Hult, A. Matamis, E. Baudoin, S. Mayer, M. Richter, Spatiotemporal flame mapping in a large-bore marine diesel engine using multiple high-speed cameras, Int. J. Engine Res. 21 (4) (2020) 622–631, doi:10.1177/1468087419853429.

[37] A.K. Jasuja, Atomization of crude and residual fuel oils, J. Eng. Gas Turbine Power 101 (2) (1979) 250–258, doi:10.1115/1.3446480.

[38] P. Jenny, D. Roekaerts, N. Beishuizen, Modeling of turbulent dilute spray combustion, 2012, doi:10.1016/j.pecs.2012.07.001.

[39] S. Karami, E.R. Hawkes, M. Talei, J.H. Chen, Edge flame structure in a turbulent lifted flame: a direct numerical simulation study, Combust. Flame 169 (2016) 110–128, doi:10.1016/j.combustflame.2016.03.006.

[40] K. Kumar, J.E. Freeh, C.J. Sung, Y. Huang, Laminar flame speeds of preheated isooctane/O_2/N_2 and n-heptane/O_2/N_2 mixtures, J. Propul. Power 23 (2) (2007) 428–436, doi:10.2514/1.24391.

[41] S. Kumar, P.J. Paul, H.S. Mukunda, Prediction of flame liftoff height of diffusion/partially premixed jet flames and modeling of mild combustion burners, Combust. Sci. Technol. 179 (10) (2007) 2219–2253, doi:10.1080/00102200701407887.

[42] C.J. Lawn, Lifted flames on fuel jets in co-flowing air, Prog. Energy Combust. Sci. 35 (2008) 1–30, doi:10.1016/j.pecs.2008.06.003.

[43] A. Lefebvre, V. McDonell, Atomization and sprays, 2017, doi:10.1016/0009-2509(90)87140-N.

[44] P.J. Linstrom, W.G. Mallard, The NIST chemistry webbook: a chemical data resource on the internet, J. Chem. Eng. Data 46 (5) (2001) 1059–1063, doi:10.1021/je000236i.

[45] H. Liu, Z. Zheng, M. Yao, P. Zhang, Z. Zheng, B. He, Y. Qi, Influence of temperature and mixture stratification on HCCI combustion using chemiluminescence images and CFD analysis, Appl. Therm. Eng. 33–34 (1) (2012) 135–143, doi:10.1016/j.applthermaleng.2011.09.026.

[46] K.M. Lyons, Toward an understanding of the stabilization mechanisms of lifted turbulent jet flames: experiments, 2007, doi:10.1016/j.pecs.2006.11.001.

[47] J. Manin, L.M. Pickett, S.A. Skeen, Toward quantitative spray measurements using high-performance high-speed video cameras, ILASS Am. (2016) 511–518.

[48] J. Manin, S.A. Skeen, L.M. Pickett, Two-color diffused back-illumination imaging as a diagnostic for time-resolved soot measurements in reacting sprays, SAE Int. J. Engines 6 (4) (2013) 1908–1921, doi:10.4271/2013-01-2548.

[49] S.K. Marley, K.M. Lyons, K.A. Watson, Leading-Edge reaction zones in lifted-Jet gas and spray flames, Flow Turbul. Combust. 72 (1) (2004) 29–47, doi:10.1023/B:APPL.0000014906.91990.4e.

[50] S.K. Marley, E.J. Welle, K.M. Lyons, W.L. Roberts, Effects of leading edge entrainment on the double flame structure in lifted ethanol spray flames, Exp. Therm. Fluid Sci. 29 (1) (2004) 23–31, doi:10.1016/j.expthermflusci.2004.01.009.

[51] C.S. Mcenally, L.D. Pfefferle, Improved sooting tendency measurements for aromatic hydrocarbons and their implications for naphthalene formation pathways, Combust. Flame 148 (2007) 210–222, doi:10.1016/j.combustflame.2006.11.003.

[52] I.A. Mulla, G. Godard, B. Renou, Instantaneous planar measurements of nitric oxide concentration in a turbulent n-heptane spray flame, Combust. Flame 208 (2019) 451–471, doi:10.1016/j.combustflame.2019.07.026.

[53] I.A. Mulla, B. Renou, Simultaneous imaging of soot volume fraction, PAH, and OH in a turbulent n-heptane spray flame, Combust. Flame 209 (2019) 452–466, doi:10.1016/j.combustflame.2019.08.012.

[54] G.D. Myers, A.H. Lefebvre, Flame propagation in heterogeneous mixtures of fuel drops and air, Combust. Flame 66 (2) (1986) 193–210, doi:10.1016/0010-2180(86)90091-X.

[55] C.V. Naik, K.V. Puduppakkam, A. Modak, E. Meeks, Y.L. Wang, Q. Feng, T.T. Tsotsis, Detailed chemical kinetic mechanism for surrogates of alternative jet fuels, Combust. Flame 158 (3) (2011) 434–445, doi:10.1016/j.combustflame.2010.09.016.

[56] K. Nakakita, M. Nagaoka, T. Fujikawa, K. Ohsawa, S. Yamaguchi, Photographic and three dimensional numerical studies of diesel soot formation process, in: SAE Technical Paper, 1990. 10.4271/902081

[57] D.B. Olson, J.C. Pickens, R.J. Gill, The effects of molecular structure on soot formation II. Diffusion flames, Combust. Flame 62 (1) (1985) 43–60, doi:10.1016/0010-2180(85)90092-6.

[58] Y. Onuma, M. Ogasawara, Studies on the structure of a spray combustion flame, Symp. (Int.) Combust. 15 (1975) 453–465, doi:10.1016/S0082-0784(75)80319-5. Elsevier

[59] Y. Onuma, T. Tsuji, M. Ogasawara, Studies on the flame structure of a spray burner, JSME 17 (112) (1974) 1296–1304, doi:10.1299/jsme1958.17.1296.

[60] M. Orain, Y. Hardalupas, Influence du combustible sur la mesure de richesse par chimiluminescence dans les flammes prémélangées, C.R. Mec. 338 (5) (2010) 241–254, doi:10.1016/j.crme.2010.05.002.

[61] C.S. Panoutsos, Y. Hardalupas, A.M. Taylor, Numerical evaluation of equivalence ratio measurement using OH* and CH* chemiluminescence in premixed and non-premixed methane-air flames, Combust. Flame 156 (2) (2009) 273–291, doi:10.1016/j.combustflame.2008.11.008.

[62] F. Payri, J.V. Pastor, J.M. Garcia-Oliver, J.M. Pastor, Contribution to the application of two-colour imaging to diesel combustion, Meas. Sci. Technol. 18 (8) (2007) 2579–2598, doi:10.1088/0957-0233/18/8/034.

[63] R. Payri, J. Gimeno, S. Cardona, S. Ayyapureddi, Experimental study of the influence of the fuel and boundary conditions over the soot formation in multihole diesel injectors using high-speed color diffused back-illumination technique, Appl. Therm. Eng. 158 (2019) 113746, doi:10.1016/J.APPLTHERMALENG.2019.113746.

[64] R. Payri, F.J. Salvador, J. Gimeno, S. Cardona, Experimental study of the influence of the boundary conditions on the atomization process in an unconfined atmospheric burner, ILASS-Europe, 2019.

[65] R. Payri, F.J. Salvador, J. Manin, A. Viera, Diesel ignition delay and lift-off length through different methodologies using a multi-hole injector, Appl. Energy 162 (2016) 541–550, doi:10.1016/j.apenergy.2015.10.118.

[66] N. Peters, Turbulent combustion, 2000, doi:10.1017/cbo9780511612701.

[67] L.M. Pickett, D.L. Siebers, Soot in diesel fuel jets: effects of ambient temperature, ambient density, and injection pressure, Combust. Flame 138 (1) (2004) 114–135, doi:10.1016/j.combustflame.2004.04.006.

[68] L.M. Pickett, D.L. Siebers, Soot formation in diesel fuel jets near the lift-off length, Int. J. Engine Res. 7 (2) (2006) 103–130, doi:10.1243/146808705X57793.

[69] L.M. Pickett, D.L. Siebers, C.A. Idicheria, Relationship between ignition processes and the lift-off length of diesel fuel jets, SAE Paper (724) (2005). doi:10.4271/2005-01-3843.

[70] G. Pinguet, D. Escudié, Experimental study of the stabilization process of a non-premixed flame via the destabilization analysis of the blue ring flame,

Exp. Therm. Fluid Sci. 31 (5) (2007) 453–460, doi:10.1016/j.expthermflusci.2006.04.014.
[71] A. Radcliffe, Section D. Fuel Injection, Design and Performance of Gas Turbine Power Plants, Princeton University Press (2015), pp. 92–118, doi:10.1515/9781400875603-008.
[72] V.M. Reddy, D. Trivedi, S. Kumar, Experimental investigations on lifted spray flames for a range of coflow conditions, Combust. Sci. Technol. 184 (1) (2012) 44–63, doi:10.1080/00102202.2011.615770.
[73] J. Réveillon, L. Vervisch, Partially premixed combustion in spray flames, Technical Report
[74] J. Reveillon, L. Vervisch, Analysis of weakly turbulent dilute-spray flames and spray combustion regimes, J. Fluid Mech 537 (2005) 317–347, doi:10.1017/S0022112005005227.
[75] D.L. Siebers, Liquid-phase fuel penetration in diesel sprays, in: SAE Technical Paper, 1998, pp. 1–23. doi:10.4271/980809.
[76] D.L. Siebers, B. Higgins, Flame lift-Off on direct-Injection diesel sprays under quiescent conditions, SAE Technical Paper (724) (2001).
[77] S.A. Skeen, J. Manin, K. Dalen, L.M. Pickett, Extinction-based imaging of soot processes over a range of diesel operating conditions, 8th US National Combustion Meeting (2013), pp. 1–13. Utah, USA
[78] D.R. Snelling, K.A. Thomson, G.J. Smallwood, Ö.L. Gülder, Two-dimensional imaging of soot volume fraction in laminar diffusion flames, Appl. Opt. 38 (12) (1999) 2478, doi:10.1364/AO.38.002478.
[79] P.B. Sunderland, S. Mortazavi, G.M. Faeth, D.L. Urban, Laminar smoke points of nonbuoyant jet diffusion flames, Combust. Flame 96 (1–2) (1994) 97–103, doi:10.1016/0010-2180(94)90161-9.
[80] K.A. Thomson, M.R. Johnson, D.R. Snelling, G.J. Smallwood, Diffuse-light two-dimensional line-of-sight attenuation for soot concentration measurements, Appl. Opt. 47 (5) (2008) 694, doi:10.1364/AO.47.000694.
[81] S. Tsushima, H. Saitoh, F. Akamatsu, M. Katsuki, Observation of combustion characteristics of droplet clusters in a premixed-spray flame by simultaneous monitoring of planar spray images and local chemiluminescence, Symp. (Int.) Combust. 27 (1998) 1967–1974, doi:10.1016/S0082-0784(98)80041-6.
[82] A. Verdier, J. Marrero Santiago, A. Vandel, G. Godard, G. Cabot, B. Renou, Local extinction mechanisms analysis of spray jet flame using high speed diagnostics, Combust. Flame 193 (2018) 440–452, doi:10.1016/j.combustflame.2018.03.032.
[83] A. Verdier, J. Marrero Santiago, A. Vandel, S. Saengkaew, G. Cabot, G. Grehan, B. Renou, Experimental study of local flame structures and fuel droplet properties of a spray jet flame, Proc. Combust. Inst. 36 (2) (2017) 2595–2602, doi:10.1016/j.proci.2016.07.016.
[84] S. Verma, S. Basu, Application of Inverse Abel Transform on flame image, Technical Report, Indian Institute of Science.
[85] H. Wang, Formation of nascent soot and other condensed-phase materials in flames, Proc. Combust. Inst. 33 (1) (2011) 41–67, doi:10.1016/j.proci.2010.09.009.
[86] L.Y. Wang, C.K. Bauer, Ö.L. Gülder, Soot and flow field in turbulent swirl-stabilized spray flames of jet A-1 in a model combustor, Proc. Combust. Inst. 37 (4) (2019) 5437–5444, doi:10.1016/j.proci.2018.05.093.
[87] Q. Wang, L. Hu, M. Zhang, F. Tang, X. Zhang, S. Lu, Lift-off of jet diffusion flame in sub-atmospheric pressures: an experimental investigation and interpretation based on laminar flame speed, Combust. Flame 161 (4) (2014) 1125–1130, doi:10.1016/j.combustflame.2013.10.021.
[88] Y. Wang, S.H. Chung, Soot formation in laminar counterflow flames, 2019. 10.1016/j.pecs.2019.05.003
[89] H. Watanabe, R. Kurose, S.M. Hwang, F. Akamatsu, Characteristics of flamelets in spray flames formed in a laminar counterflow, Combust. Flame 148 (4) (2007) 234–248, doi:10.1016/j.combustflame.2006.09.006.
[90] X. Wei, H. Yong, Improved semiempirical correlation to predict sauter mean diameter for pressure-Swirl atomizers, J. Propul. Power 30 (6) (2014) 1628–1635, doi:10.2514/1.B35238.
[91] N. Weinberg, J.B. Greenberg, On blow-out and lift-off of laminar jet spray diffusion flames, Combust. Sci. Technol. 188 (11–12) (2016) 1760–1776, doi:10.1080/00102202.2016.1211858.
[92] N. Weinberg, J.B. Greenberg, Polydisperse effects in jet spray flames, Combust. Theor. Model. 22 (1) (2018) 71–90, doi:10.1080/13647830.2017.1376117.
[93] F. Xu, P.B. Sunderland, G.M. Faeth, Soot formation in laminar premixed ethylene/air flames at atmospheric pressure, Combust. Flame 108 (4) (1997) 471–493, doi:10.1016/S0010-2180(96)00200-3.
[94] Y. Xu, C.-f.F. Lee, Forward-illumination light-extinction technique for soot measurement, Appl. Opt. 45 (9) (2006) 2046, doi:10.1364/AO.45.002046.
[95] M.G. Yeganeh, Effects of preheated combustion air on laminar coflow diffusion flames under normal and microgravity conditions, University of Maryland, College Park,, 2005 Ph.D. thesis.
[96] T.L. Yelverton, W.L. Roberts, Effect of dilution, pressure, and velocity on smoke point in laminar jet flames, Combust. Sci. Technol. 180 (7) (2008) 1334–1346, doi:10.1080/00102200801931570.
[97] I. Zahmatkesh, M. Moghiman, Effect of liquid fuel droplet size on soot emission from turbulent spray flames, Iran. J. Sci. Technol. Trans. B Eng. 30 (3) (2006) 339–351.
[98] H. Zhao, N. Ladommatos, Optical diagnostics for soot and temperature measurement in diesel engines, Technical Report, 1998.